Communications in Physics, Vol. 29, No. 1 (2019), pp. 1-33
DOI:10.15625/0868-3166/29/1/13185

REVIEW PAPER

CONTROLLABLE OPTICAL PROPERTIES OF MULTIPLE ELECTROMAGNETICALLY INDUCED TRANSPARENCY IN GASEOUS ATOMIC MEDIA

BANG NGUYEN HUY†, DOAI LE VAN AND KHOA DINH XUAN

Vinh University, 182 Le Duan street, Vinh City, Vietnam

†*E-mail:* bangnh@vinhuni.edu.vn

Received 9 October 2018
Accepted for publication 29 November 2018
Published 31 January 2019

Abstract. *The advent of electromagnetically induced transparency (EIT) offered a new coherent material with exotic and controllable optical properties. Extension from single to multiple EIT is of current interest because it gains advantages in multi-channel optical communication, waveguides for optical signal processing and multi-channel quantum information processing. In this work, we review recent research works concerning multiple EIT and some related applications such as controlling group velocity of light, giant Kerr nonlinearity, optical bistability. The special attention of the review is also on analytical interpretations of the results to give physics insight and suitable applications. From an experimental point of view, the latest development for measuring multiple EIT spectrum and its dispersion in hot medium is presented and compared to the theoretical analytical representations.*

Keywords: effects of atomic coherence.

Classification numbers: 42.50.Gy; 42.65.-k; 42.65.Pc.

©2019 Vietnam Academy of Science and Technology

I. INTRODUCTION

The EIT is a quantum interference effect which makes a resonance medium transparent and steeper dispersion for a probe light field under induction of a strong coupling light field. The effect was proposed theoretically in 1989 [1] and experimentally verified in 1991 [2]. Since then, the EIT has attracted much studies in atomic/molecular systems [3–14] and quantum well/dot systems [15–19] due to its unusual optical properties and promises for potential applications, such as lasing without inversion [20], high resolution spectroscopy [21], nonlinear optics at low light levels [22], giant Kerr nonlinearity [23–26], and optical bistability (OB) [27]. In addition to the reduction of the resonant absorption, modification of refractive index of the EIT medium was also studied theoretically [28, 29] and experimentally [8, 30]. It has been shown that a very steep slope of the refractive index profile can slow down group velocity of light [31], even stop and storage of light pulse in the EIT medium [32]. These aspects deliver several potential applications, *e.g*., lossless propagation of light pulse [33–35], all-optical switching [36–38], quantum storage devices, logic gates and the generation of photonic qubits [39, 40], and so on.

In the early years of EIT study, three-level configurations were the main objects which give single-window EIT signature [3–19]. It is worthy to mention here that the linear and nonlinear susceptibilities of such single-window EIT medium have been well understood and promoted significant progress in the EIT related applications [20–40]. From the practical perspective, extension from single- to multi-window EIT is of current interest in multi-channel optical communication, waveguides for optical signal processing and multi-channel quantum information processing. A possible way for the generation of multiple EIT is to use additional controlling fields to excite various multi-level atomic configurations, such as N-level cascade-type configuration [41], (N+1)-level lambda-type configuration [42], N-type configuration [43], K-type configuration [44], inverted Y-type configuration [45], and M-type configuration [46], etc. Other studies on the EIT in the multi-level system based on velocity selection [47–50], in nanofiber [51, 52], and in the presence of the magnetic field [53–55] are proposed most recently. Some research groups used such controlling fields to control the optical properties of EIT medium at multiple frequencies, *e.g*., manipulation of the group velocity [42, 46, 56-58], Kerr nonlinearity [59–61], OB [62–65], all-optical switching [66–69], and controllable entanglement of lights in a five-level system [70], etc.

Another simple way for the generation of multiple EIT is to use only a controlling field to couple simultaneously several closely-spaced hyperfine levels which was experimentally demonstrated and numerically simulated for a five-level cascade scheme of cold ^{85}Rb atoms [71, 72]. The excitation scheme has several advantages. The first advantage is the possibility to generate simultaneously three EIT windows, which can simultaneously support slow group velocities for more probe pulses at different frequencies. As discussed in [73], slowed-light is obtained at different frequencies corresponding to EIT windows that is advantageous to efficiently produce the quantum entanglement. The second advantage is the possibility to choose the uppermost excited states as the Rydberg states having long life-time which increase significantly atomic coherence [58].

Although the numerical simulations on the EIT spectrum in [71, 72] were helpful to explain experimental observation, there is still a lack of analytical representation of EIT spectrum which is important for various applications. In order to overcome this lack, Bang and co-workers have

recently developed an analytical method to represent the EIT spectrum [74–76]. Such analytical model supports several interesting works concerning giant Kerr nonlinearity [77], OB [78], generating optical nano-fiber (ONF) for guiding entangled beams [79], slowed multi-frequency light [80, 81], and lossless propagation of light pulse [34, 35].

In this work, we review the research works concerning the generation of the multiple EIT and related applications. The paper is organized as follows: Sec. I briefs an overview of the EIT and its applications. Sec. II is devoted to physics of single EIT with two controllable properties, absorption and dispersion. Sec. III presents physics of multiple EIT by using an analytical model and a latest experimental observation in a hot atomic medium. Controllable giant Kerr nonlinearity and group velocity of the EIT medium are presented in Sec. IV and Sec. V, respectively. A fascinating application of the giant Kerr of multiple EIT media is optical bistability which is presented in Sec.VI. Finally, we conclude the topic with a perspective of multi-window EIT in Sec. VII.

II. PHYSICS OF SINGLE EIT

A fascinating aspect of the coherent interaction between electromagnetic field and atom is quantum interference of probability amplitudes between transition channels within an atomic system that modifies optical response of the atomic medium. The interference leads to either an enhancement (constructive interference) or a complete cancellation (destructive interference) of the total transition probability. The cancellation of total transition probability leads to an elimination of resonant absorption which is called the EIT [1, 2] whereas the remaining case leads to an enhancement of absorption which is called as electromagnetically induced absorption (EIA) [82]. Physically, to create the interference effect, one needs at least two transition channels in an atomic system with a common level that is induced by a probe laser field ω_p and a coupling laser field ω_c, as in Fig. 1 [83]. The dipole allowed transitions are between states $|1\rangle$ and $|2\rangle$ and between states $|2\rangle$ and $|3\rangle$. The EIT has been extensively studied in all three of the three-level configurations [3–14].

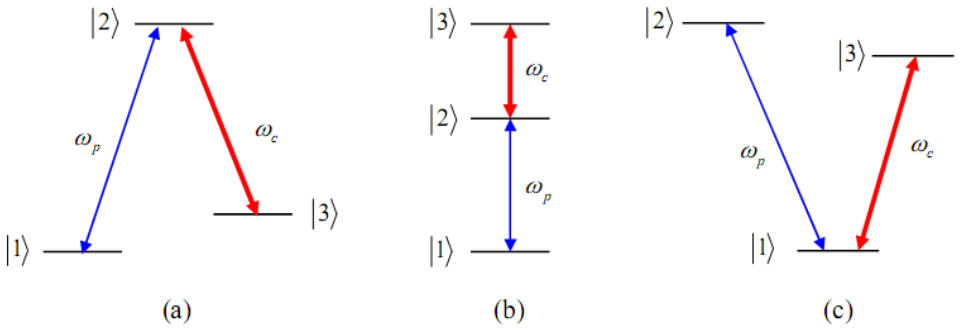

Fig. 1. Three-level excited configurations: (a) lambda, (b) cascade, and (c) V.

The theory of EIT for lambda-, cascade - and V-type configurations has been well documented in Refs. [3-14]. In the framework of the semiclassical theory, using the dipole and rotating wave approximations, the evolution of the atom-field system can be described by the following

Liouville equation [26]:

$$\dot{\rho} = -\frac{i}{\hbar}[H, \rho] + \Lambda\rho, \tag{1}$$

where H, ρ, and Λ stand for the total Hamiltonian, density matrix operator, and relaxation operator in the atomic system, respectively. Under the rotating field and electric dipole approximations, and using perturbation technique, the first-order density matrix element corresponding to the probe transition is given by [26]:

$$\rho_{21}^{(1)} = \frac{-\frac{i}{2}\Omega_p}{\gamma_{21} - i\Delta_p + \frac{(\Omega_c/2)^2}{\gamma_{31} - i(\Delta_p - \Delta_c)}}. \tag{2}$$

The first-order susceptibility $\chi^{(1)}$ for the probe light field is represented by

$$\chi^{(1)} = -2\frac{Nd_{21}}{\varepsilon_0 E_p}\rho_{21}^{(1)} = \frac{iNd_{21}^2}{\varepsilon_0\hbar}\frac{1}{\gamma_{21} - i\Delta_p + \frac{(\Omega_c/2)^2}{\gamma_{31} - i(\Delta_p - \Delta_c)}}. \tag{3}$$

The absorption and dispersion of the medium for the probe field can be obtained from the real ($\chi\prime$) and imaginary (χ?) parts of the complex susceptibility, namely [26]

$$\chi = \chi' + i\chi'' = \frac{Nd_{21}^2}{\varepsilon_0\hbar}\left(\frac{-\Delta_p + \frac{A_{23}}{\gamma_{31}}}{\left(-\Delta_p + \frac{A_{23}}{\gamma_{31}}\right)^2 + \left(\gamma_{21} + \frac{A_{23}}{\Delta_p - \Delta_c}\right)^2} + i\frac{\gamma_{21} + \frac{A_{23}}{\Delta_p - \Delta_c}}{\left(-\Delta_p + \frac{A_{23}}{\gamma_{31}}\right)^2 + \left(\gamma_{21} + \frac{A_{23}}{\Delta_p - \Delta_c}\right)^2}\right), \tag{4}$$

where A_{23} is an effective coupling parameter given by

$$A_{23} = \frac{\gamma_{31}(\Delta_p - \Delta_c)}{\gamma_{31}^2 + (\Delta_p - \Delta_c)^2}\left(\frac{\Omega_c}{2}\right)^2. \tag{5}$$

The absorption and the dispersion coef?cients are given by

$$\alpha = \frac{\omega_p n_0 \chi''}{c} = \frac{\omega_p n_0 N d_{21}^2}{c\varepsilon_0\hbar}\frac{\gamma_{21} + \frac{A_{23}}{\Delta_p - \Delta_c}}{\left(-\Delta_p + \frac{A_{23}}{\gamma_{31}}\right)^2 + \left(\gamma_{21} + \frac{A_{23}}{\Delta_p - \Delta_c}\right)^2}, \tag{6}$$

$$n = \frac{\omega_p n_0 \chi'}{2c} = \frac{\omega_p n_0 N d_{21}^2}{2c\varepsilon_0\hbar}\frac{-\Delta_p + \frac{A_{23}}{\gamma_{31}}}{\left(-\Delta_p + \frac{A_{23}}{\gamma_{31}}\right)^2 + \left(\gamma_{21} + \frac{A_{23}}{\Delta_p - \Delta_c}\right)^2}, \tag{7}$$

where n_0 is the background index of refraction and c is the speed of light in the vacuum.

For the case of atomic medium of ^{87}Rb, the states, $|1\rangle$, $|3\rangle$, $|2\rangle$ can be chosen as $5S_{1/2}(F = 1)$, $5S_{1/2}(F = 2)$ and $5P_{1/2}(F\prime = 2)$, respectively. The atomic parameters are [26]: $N = 5\times10^{11}$ atoms/cm^3, $d_{21} = 1.6\times10^{-29}$ C.m, and $\omega_p = 3.77\times10^8$ MHz. Using the expressions (6) and (7) the absorption (a) and dispersion (b) are plotted as in Fig. 2 in which the solid line is for coupling laser on ($\Omega_c = 10$ MHz) while dashed line stands for the coupling laser off ($\Omega_c = 0$).

In the presence of coupling laser field, the resonant absorption of the medium for the probe light vanished (forming a *transparent spectral region* called as *EIT window*) as described by the solid line in Fig. 2(a). To explain this interference, we use the lambda configuration as shown in Fig. 1(a). There are two transition channels between states $|1\rangle$ and $|2\rangle$: the first one is the direct

path from the state $|1\rangle$ to state $|2\rangle$ caused by the probe laser field Ω_p; the second one is the indirect path from state $|1\rangle$ to state $|2\rangle$ then back to state $|3\rangle$ and then return to the state $|2\rangle$ that is induced by the coupling laser field Ω_c. Due to quantum destructive interference between the probability amplitudes of two transition channels, the total probability amplitude for the probe laser vanishes, i.e., this yields a transparency region for the probe laser field (EIT window), as the solid line in Fig. 2(a). Along with vanished absorption, on the dispersive profile appears a normal dispersion with its height and slope being radically modified, as shown in Fig. 2(b). Such modification has delivered several fascinating applications. For further comprehensive reviews on such single EIT, we refer readers to the works done by Fleischhauer *et al*. [83] and Marangos [84].

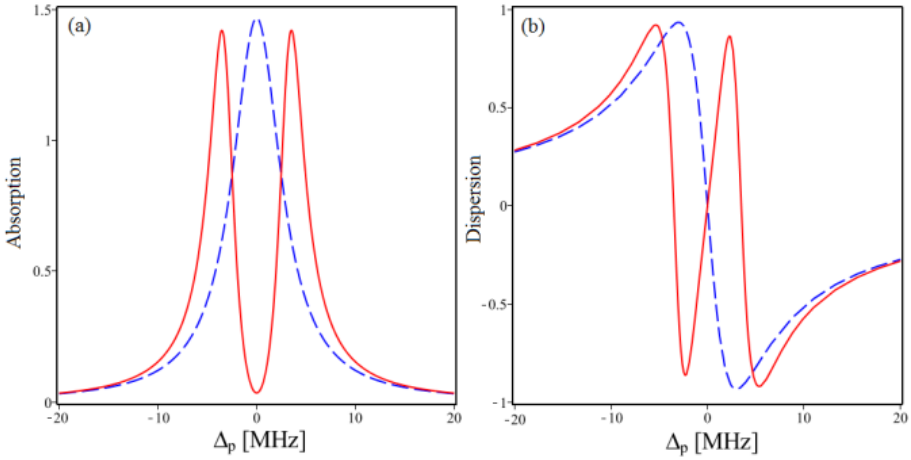

Fig. 2. Absorption (a) and dispersion (b) for the probe field with (solid line) or without (dashes line).

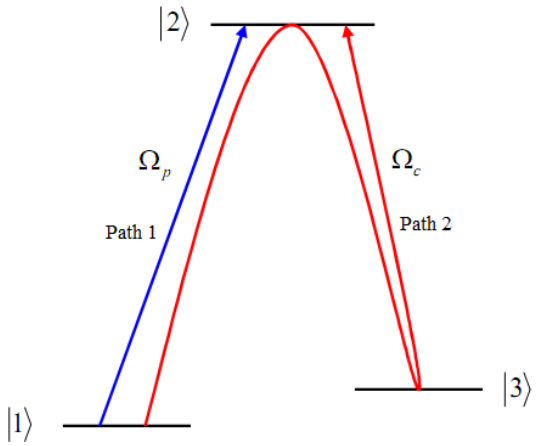

Fig. 3. Interference between two transition pathways from the ground state $|1\rangle$ to the excited state $|2\rangle$.

III. MULTIPLE EIT

III.1. Analytical representation

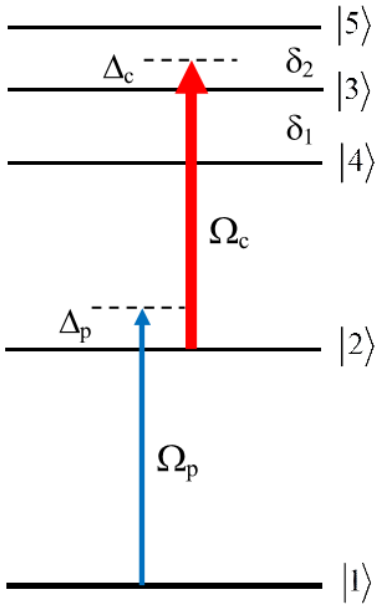

Fig. 4. Five-level cascade-type excitation system.

We consider a five-level cascade-type system interacting with two laser fields as in Fig. 4. A weak probe laser field (with frequency ω_p and Rabi frequency Ω_p) drives the transition $|1\rangle \leftrightarrow |2\rangle$, whereas an intense coupling laser field (with frequency ω_c and Rabi frequency Ω_c) couples simultaneously transitions between the state $|2\rangle$ and three closely-spacing states $|3\rangle$, $|4\rangle$ and $|5\rangle$. Both probe and coupling fields counter-propagate through the medium. We denote by δ_1 and δ_2 the frequency separations between the levels $|3\rangle - |4\rangle$ and $|5\rangle - |3\rangle$, respectively. The frequency detuning of the probe and coupling lasers are defined respectively as:

$$\Delta_p = \omega_p - \omega_{21}, \ \Delta_c = \omega_c - \omega_{32}. \tag{8}$$

Under the first-order perturbation, the density matrix equations can be used to derive the linear susceptibility as [74]

$$\chi^{(1)} = \frac{Nd_{21}^2}{\varepsilon_0 \hbar}\left(\frac{A}{A^2+B^2} + i\frac{B}{A^2+B^2}\right), \tag{9}$$

where $A$and B are real parameters given by:

$$A = -\Delta_p + \frac{A_{32}}{\gamma_{31}} + \frac{A_{42}}{\gamma_{41}} + \frac{A_{52}}{\gamma_{51}}, \tag{10}$$

$$B = \gamma_{21} + \frac{A_{32}}{\Delta_p + \Delta_c} + \frac{A_{42}}{\Delta_p + \Delta_c + \delta_1} + \frac{A_{52}}{\Delta_p + \Delta_c - \delta_2}, \tag{11}$$

$$A_{32} = \frac{\gamma_{31}(\Delta_p + \Delta_c)}{\gamma_{31}^2 + (\Delta_p + \Delta_c)^2} a_{32}^2 (\Omega_c/2)^2, \tag{12}$$

$$A_{42} = \frac{\gamma_{41}(\Delta_p + \Delta_c + \delta_1)}{\gamma_{41}^2 + (\Delta_p + \Delta_c + \delta_1)^2} a_{42}^2 (\Omega_c/2)^2, \tag{13}$$

$$A_{52} = \frac{\gamma_{51}(\Delta_p + \Delta_c - \delta_2)}{\gamma_{51}^2 + (\Delta_p + \Delta_c - \delta_2)^2} a_{52}^2 (\Omega_c/2)^2, \tag{14}$$

where $a_{32} = d_{32}/d_{32}$, $a_{42} = d_{42}/d_{32}$, and $a_{52} = d_{52}/d_{32}$ are the relative transition strengths of the three transitions from the three hyperfine sublevels $|3\rangle$, $|4\rangle$ and $|5\rangle$ to level $|2\rangle$.

According to the Kramer-Kronig relation, the dispersion and absorption coefficients of the medium can be determined by [74]:

$$n = \frac{\omega_p n_0 \chi'}{2c} = \frac{\omega_p n_0 N d_{21}^2}{2c\varepsilon_0 \hbar} \frac{A}{A^2 + B^2}, \tag{15}$$

$$\alpha = \frac{\omega_p n_0 \chi''}{c} = \frac{\omega_p n_0 N d_{21}^2}{c\varepsilon_0 \hbar} \frac{B}{A^2 + B^2}. \tag{16}$$

In expressions (12), (13), and (14), the coefficient A_{k2} (k = 3, 4, 5) is defined as the *effective coupling parameter* between the states $|2\rangle$ and $|k\rangle$ under induction of the coupling laser light. The simultaneously coupling gives rise to three transparent windows. In order to visualize dependence of EIT spectra on intensity and frequency of the coupling light, α and n are plotted using the following parameters [74]: γ_{21}= 6 MHz; $\gamma_{32} = \gamma_{42} = \gamma_{52} = \gamma$ = 0.97 MHz; N = 10^{14} atom/m^3; d_{21}= 2.5×10^{-29} C.m; $\delta_1 = 9$ MHz; $\delta_2 = 7.6$ MHz; and a_{42}: a_{32}: a_{52} = 1.46:1:0.6. Fig. 5 shows a three-window EIT signature when increasing coupling laser intensity. Furthermore, distances between the centers of the EIT windows are respectively equal to the frequency separations between the hyperfine levels $|3\rangle - |4\rangle$ and $|5\rangle - |3\rangle$. These window separations can be explained by the two-photon resonance condition for the probe and coupling laser light fields, particularly at the locations Δ_p = -Δ_c = 0, Δ_p = -(Δ_c + δ_1) = -9 MHz and Δ_p = -(Δ_c - δ_2) = 7.6 MHz. Furthermore, the width and depth (thus dispersion slop) of the EIT windows increase with the increase in coupling light intensity.

The depth of EIT windows corresponding to effective coupling parameter A_{42}, A_{32} and A_{52} is calculated as

$$R_{32}|_{\Delta_p+\Delta_c=0} = \left(1 - \frac{B_3}{A_3^2 + B_3^2}\gamma_{21}\right) \times 100\%, \tag{17}$$

$$R_{42}|_{\Delta_p+\Delta_c+\delta_1=0} = \left(1 - \frac{B_4}{A_4^2 + B_4^2}\gamma_{21}\right) \times 100\%, \tag{18}$$

$$R_{52}|_{\Delta_p+\Delta_c-\delta_2=0} = \left(1 - \frac{B_5}{A_5^2 + B_5^2}\gamma_{21}\right) \times 100\%, \tag{19}$$

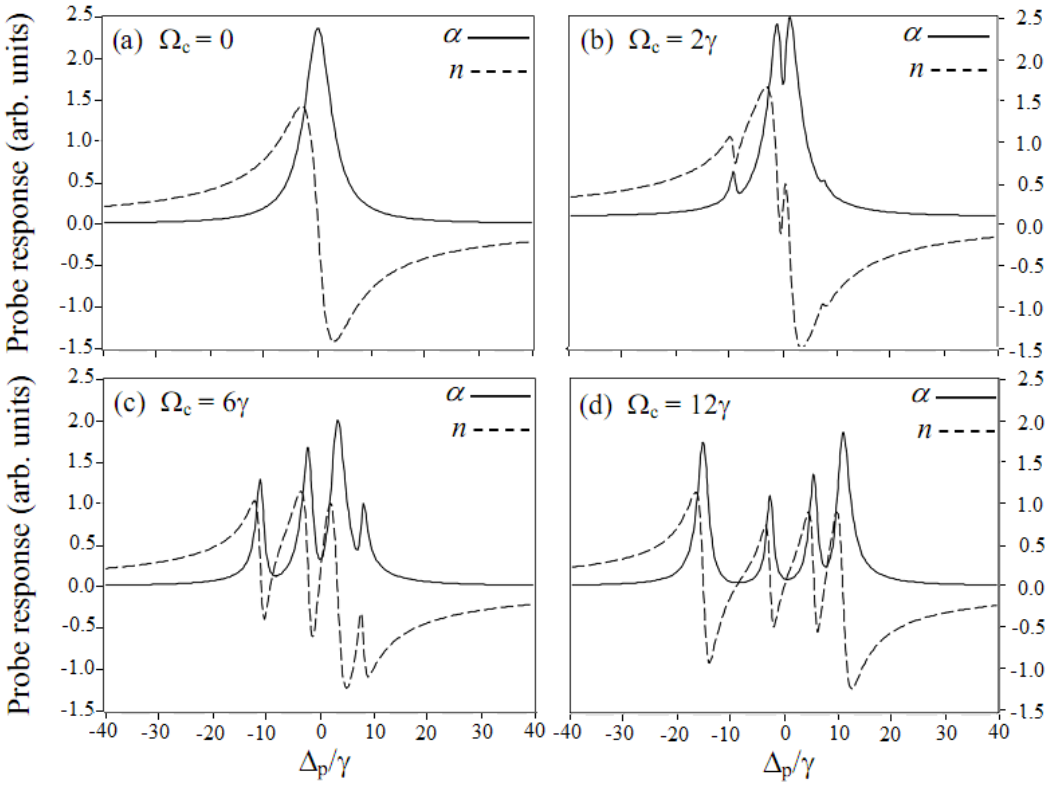

Fig. 5. Variation of the absorption (solid-line) and dispersion (dashed-line) at particular values of coupling Rabi frequency Ω_c when $\Delta_c = 0$ [74].

where

$$A_3 = \frac{\delta_1 a_{42}^2(\Omega_c/2)^2}{\gamma_{31}^2+\delta_1^2} - \frac{\delta_2 a_{52}^2(\Omega_c/2)^2}{\gamma_{31}^2+\delta_2^2}, \tag{20}$$

$$B_3 = \gamma_{21} + \frac{a_{32}^2(\Omega_c/2)^2}{\gamma_{31}} + \frac{\gamma_{31} a_{42}^2(\Omega_c/2)^2}{\gamma_{31}^2+\delta_1^2} + \frac{\gamma_{31} a_{52}^2(\Omega_c/2)^2}{\gamma_{31}^2+\delta_2^2}. \tag{21}$$

$$A_4 = -\frac{\delta_1 a_{32}^2(\Omega_c/2)^2}{\gamma_{41}^2+\delta_1^2} - \frac{(\delta_1+\delta_2) a_{52}^2(\Omega_c/2)^2}{\gamma_{41}^2+(\delta_1+\delta_2)^2}, \tag{22}$$

$$B_4 = \gamma_{21} + \frac{\gamma_{41} a_{32}^2(\Omega_c/2)^2}{\gamma_{41}^2+\delta_1^2} + \frac{a_{42}^2(\Omega_c/2)^2}{\gamma_{41}} + \frac{\gamma_{41} a_{52}^2(\Omega_c/2)^2}{\gamma_{41}^2+(\delta_1+\delta_2)^2}, \tag{23}$$

$$A_5 = \frac{\delta_2 a_{32}^2(\Omega_c/2)^2}{\gamma_{51}^2+\delta_2^2} + \frac{(\delta_1+\delta_2) a_{42}^2(\Omega_c/2)^2}{\gamma_{51}^2+(\delta_1+\delta_2)^2}, \tag{24}$$

$$B_5 = \gamma_{21} + \frac{\gamma_{51} a_{32}^2(\Omega_c/2)^2}{\gamma_{51}^2+\delta_2^2} + \frac{\gamma_{51} a_{42}^2(\Omega_c/2)^2}{\gamma_{51}^2+(\delta_1+\delta_2)^2} + \frac{a_{52}^2(\Omega_c/2)^2}{\gamma_{51}}. \tag{25}$$

Variation of the depths versus Ω_c is plotted in Fig. 6, where one can see a strongest and weakest efficiency of R_{EIT} for the windows corresponding to the effective coupling parameters A_{42} and A_{52}, respectively. This behaviour is due to A_{k2} ($k = 3, 4, 5$) which is linearly proportional to the coupling strength a_{k2}, in which a_{42}:a_{32}:a_{52} =1.46:1:0.6.

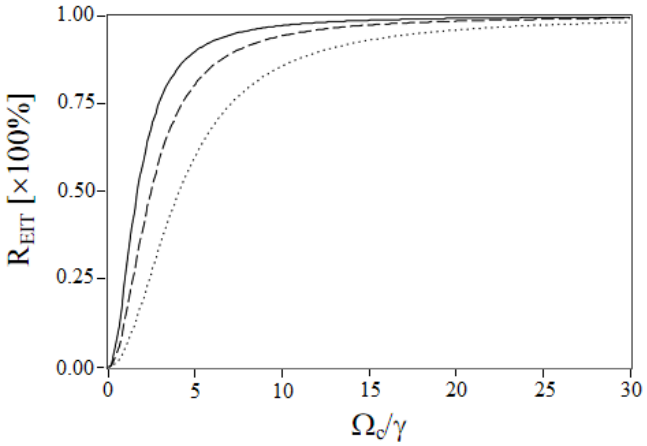

Fig. 6. Variation of R_{EIT} on coupling intensity for the three windows corresponding to the effective coupling parameter A_{42} (solid-line), A_{32}(dashed line), and A_{52} (dotted-line) [74].

The influence of the coupling frequency detuning on the EIT spectrum is shown in Fig. 7, where coupling frequency is on resonance with $|2\rangle - |3\rangle$ and $|2\rangle - |5\rangle$ transitions, which corresponds to Δ_c = -9γ and Δ_c = 7.6γ, respectively. From the figure one can see that location of the transparent windows can be controlled with the variation of the coupling frequency detuning.

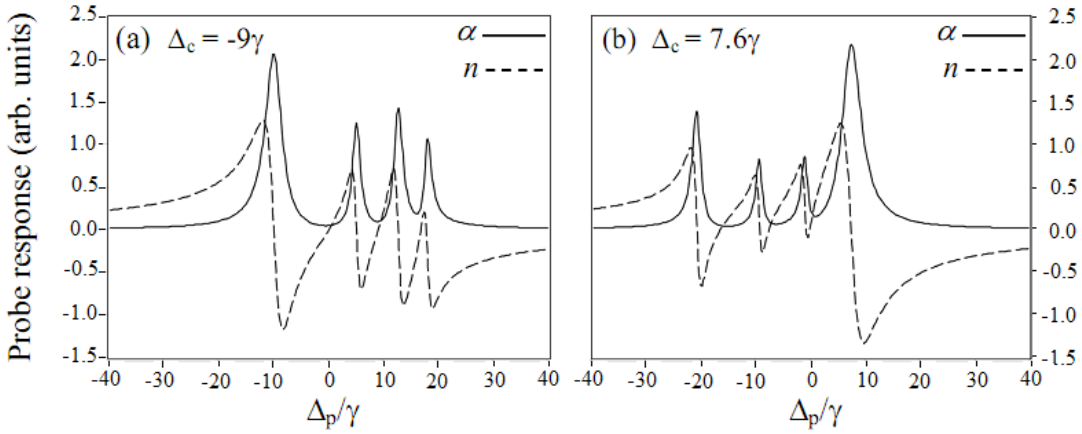

Fig. 7. Location of EIT windows at Δ_c = -9γ (a) and Δ_c = 7.6γ (b) when $\Omega_c = 12\gamma$ [74].

In the presence of Doppler effect, an atom with velocity v moving towards the probe beam will therefore "see" a frequency up-shift (by $\omega_p v/c$) and down-shift (by $-\omega_c v/c$) for the probe

and coupling lights, respectively. The frequency detunings are therefore modified to

$$\Delta_p = \omega_p - \omega_{21} + \omega_p v/c; \quad \Delta_c = \omega_c - \omega_{32} - \omega_c v/c. \tag{26}$$

The susceptibility is integrated over the velocity v from - ∞ to +∞, given by [75]:

$$\chi = \int_{-\infty}^{+\infty} \chi(v) dv = \frac{iN_0 d_{21}^2 \sqrt{\pi}}{\varepsilon_0 \hbar \left(\frac{\omega_p u}{c}\right)} e^{z^2} \left[1 - erf(z)\right], \tag{27}$$

where $erf(z)$ is the error function with a complex argument z:

$$z = \frac{c}{\omega_p u}(B + iA) \tag{28}$$

where A and B are defined by Eq. (10) and Eq. (11), respectively. By splitting the imaginary and real parts of the susceptibility in Eq. (27), the dispersion and absorption coefficients for the probe light can be determined. From these results one can consider influences of Doppler-effect on EIT spectra by simply plotting the absorption coefficient at different values of T, as shown in Fig. 8. Here we can see reduction of depths and widths of the EIT windows with increasing of temperature. The reason for this tendency is due to reduction of atomic coherence with increasing atomic motion.

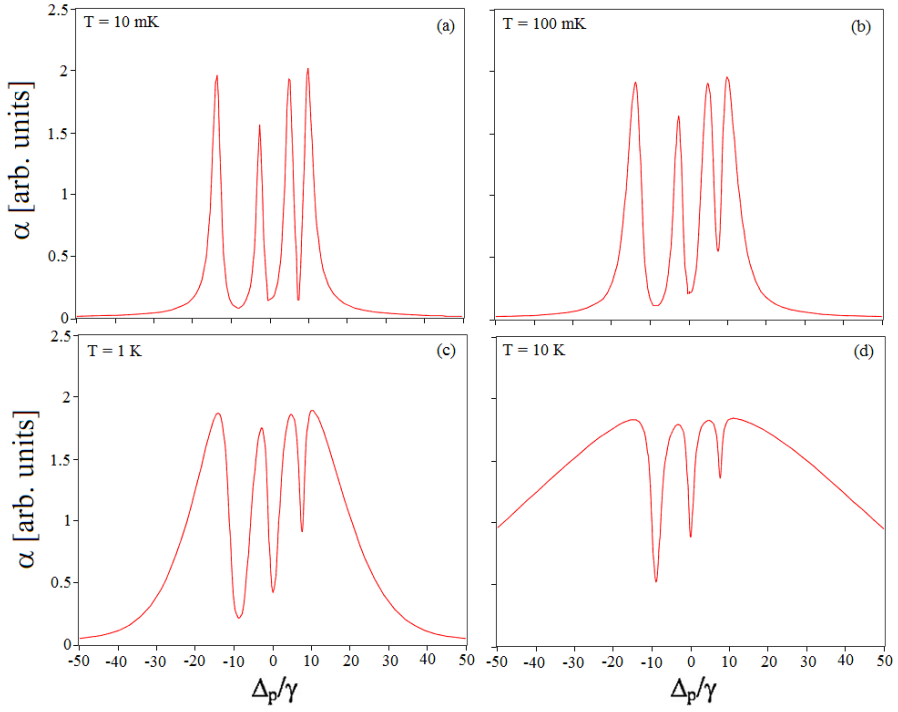

Fig. 8. Plot of absorption at different temperatures T = 10mK (a); 100mK (b); 1K (c); and 10K (d). The parameters of the coupling field are fixed at$\Delta_c = 0$ and $\Omega_c = 10\gamma$[75].

III.2. Experimental realization

After the theoretical predictions, the multiple EIT in room temperature was realized by Bang and co-workers [76]. In this experiment, the ^{85}Rb atomic gaseous sample is produced in a Rb-cell with a temperature controller. Two single-mode extended-cavity diode lasers DL1 and DL2 (with beam diameter 4mm, linewidth $\approx$1 MHz, and operating around 780 nm wavelength) are used to excite transitions on the D_2manifold of ^{85}Rb atomic system. Here, the coupling laser DL2 is used to induce EIT effect in the sample. The strong coupling beam with a fixed frequency ω_c(and Rabi frequency Ω_c) couples simultaneously the hyperfine ground state $5S_{1/2}$ ($F = 3$) with the three excited states $5P_{3/2}$ ($F' = 2, 3, 4$), whereas the weak probe beam with frequency ω_p (and Rabi frequency Ω_p) scans over same transitions from the $5S_{1/2}$ ($F = 3$) state to $5P_{3/2}$ ($F' = 2, 3, 4$) states. We denote by δ_1 and δ_2 the frequency separations between the $|2\rangle - |3\rangle$ levels and $|3\rangle - |4\rangle$ levels, respectively.

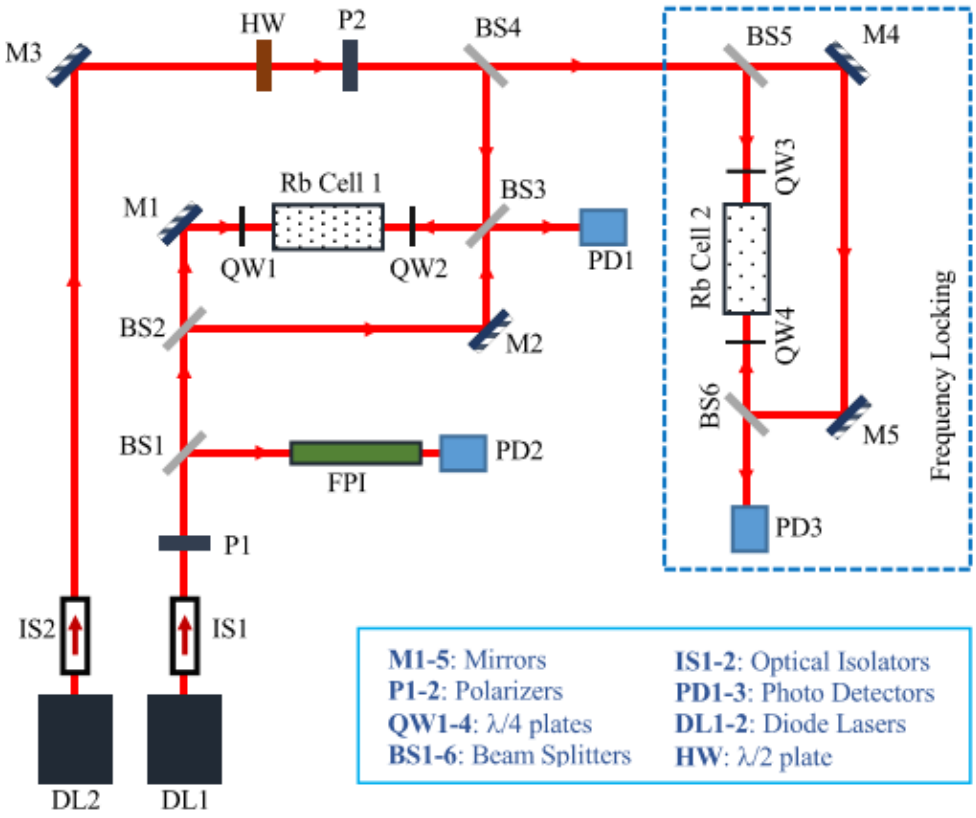

Fig. 9. Optical layout of the experimental arrangement: two diode lasers DL_1 and DL_2 are used to deliver probe and coupling lights, respectively. The dashed-border indicates a saturation spectroscopy setup for locking frequency of the coupling laser DL2 [76].

In a brief description of the setup, a small part of the laser beam DL1 is split by a beam splitter BS1 into a Fabry-Pérot interferometer – FPI (with a free-spectral range, FRS = 380 MHz) for calibration of observed spectrum, whereas the remaining one is directed to a second beam splitter (BS2), which is the entrance of a Mach-Zehnder interferometer (MZI). The MZI consists of two 50% beam splitters (BS2 and BS3) and two dielectric mirrors (M1 and M2). Each mirror or beam splitter of the MZI is mounted on a 3-axis micro-translation stage to perform a precise control of optical paths. The length of each arm of the MZI is about 20 cm, both arms are arranged so that difference of their lengths is much smaller than 1.5 cm. The Rb cell with two quarter-waveplates, QW1 and QW2 (at both ends of the cell), are placed in the second arm of the MZI. The output beam of the DL2 laser is split in two parts, the first one is directed to the Rb cell as the coupling light to induce EIT effect, and the second part is directed to a saturated absorption spectroscopic setup (within the dashed border in Fig. 9) to lock frequency of the coupling laser to a hyperfine transition.

Whenever absorption spectrum being measured, the fist arm of the MZI is blocked to avoid influence of interference on the recorded absorption spectrum. We used combination of a half-wave plates and polarizers to control intensity of the coupling and probe lights. In the measurements, the power of the probe light is reduced to few μW whereas the intensity of the coupling light is changed from few tens mW. Both probe and FPI signals are recorded simultaneously by two photodiodes PD1 and PD2, respectively. Frequency of the coupling laser is tuned resonantly to the transition $5S_{1/2}(F=3) \leftrightarrow 5P_{3/2}(F'=3)$ while the probe laser is scanned over the transitions $5S_{1/2}(F=3) \leftrightarrow 5P_{3/2}(F'=2,3,4)$. The temperature of a rubidium vapor cell is stabilized at T = 300K. The absorption and dispersion profiles for various coupling intensities are shown as in Fig. 10, where the left and right columns represent the experimental and theoretical spectra, respectively. In the theoretical simulations, the atomic parameters are chosen [76] as $\delta_1 = 63.4$ MHz; $\delta_2 = 120.6$ MHz; $\gamma_{21} = \gamma_{31} = \gamma_{41} = \gamma_{51} = 7.5$ MHz.

Figures 10(a) and 10(d) show the probe absorption and dispersion spectra without the coupling light ($\Omega_c = 0$). In this case, we see a Lorentzian absorption and its dispersion profile. When the coupling power is increased to 3.5 mW which corresponds to a value of Rabi frequency $\Omega_c = 70$ MHz (Fig. 10(b) and Fig. 10(e), the absorption spectrum apparently exhibits two EIT windows whereas the dispersion is modified in the regions of each EIT window. By increasing the coupling power up to 12 mW, which corresponds to $\Omega_c = 130$ MHz, a third EIT window occurs (the window on the right of Fig. 10(c) and Fig. 10(f). The third window occurs only at higher power of the coupling light because of the relative transition strength a_{41} corresponding to this window is quite small (a_{21}: a_{31}: $a_{41} = 0.8 : 1 : 0.3$). The frequency separations between the three EIT windows are 63.4 MHz and 120.6 MHz as same as the separations δ_1 and δ_2, respectively. By comparing Fig. 34a with Fig. 34c one can see a basic modification of dispersion under the EIT effect.

When the coupling laser is tuned to resonance with the transition $|1\rangle \leftrightarrow |3\rangle$ while its power is fixed at 42 mW (corresponds to Ω_c = 240 MHz), the measured absorption for various values of temperature is indicated in Fig. 11. It is shown that growing of temperature leads to lower EIT depth and narrower EIT width. The physical reasons to explain this tendency are attributed to reduction of atomic coherence as growing thermal atomic motion, and growing of atomic density as heating the Rb cell over the melting point of Rb (about 312 Kelvin [76]).

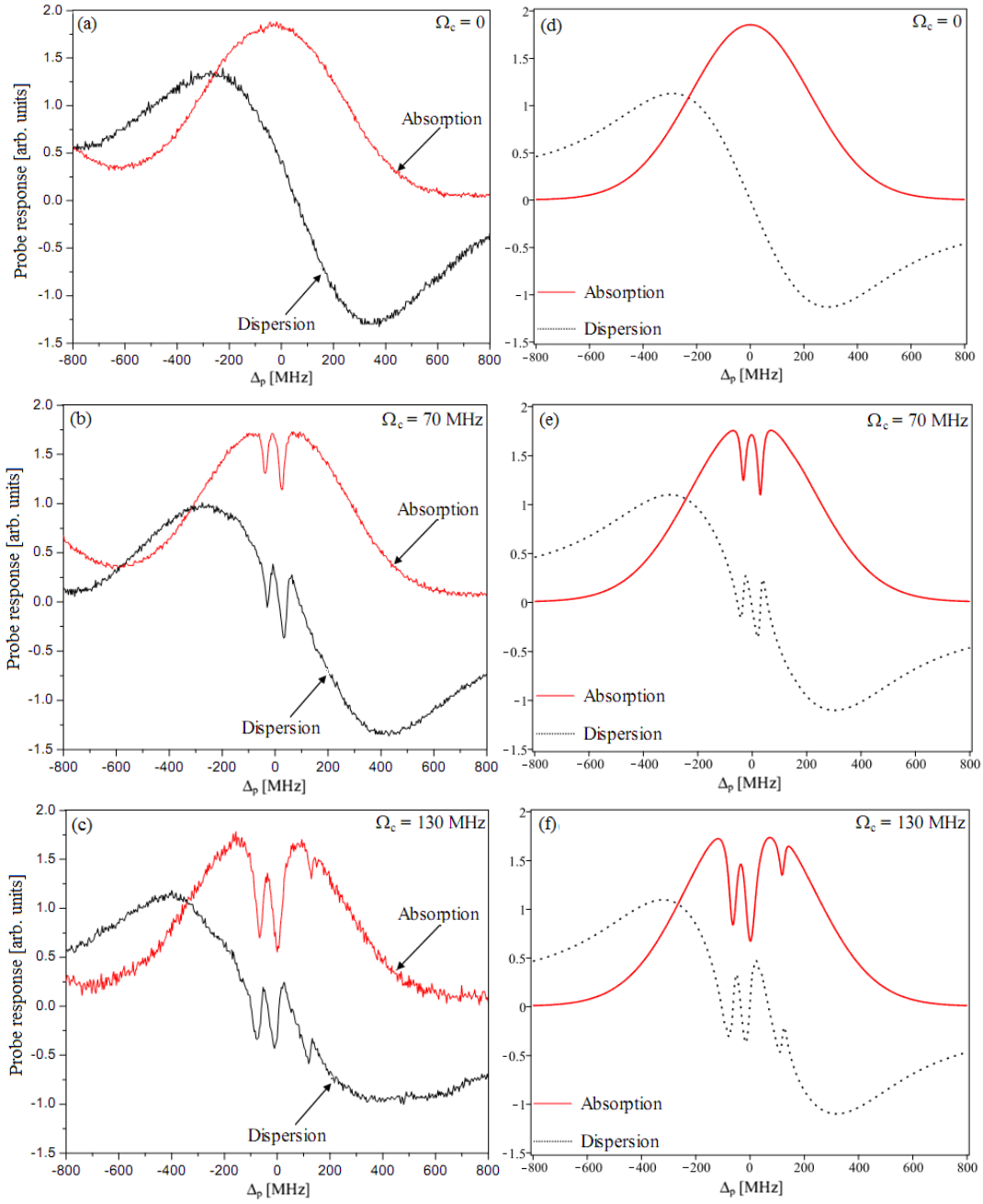

Fig. 10. Experimental observations (*left*) and theoretical simulations (*right*) of the absorption (*solid curve*) and dispersion (*dotted curve*) spectra of the probe light for various coupling intensities Ω_c (indicated in figures) when frequency detuning $\Delta_c = 0$ and $T =$ 300 K [76].

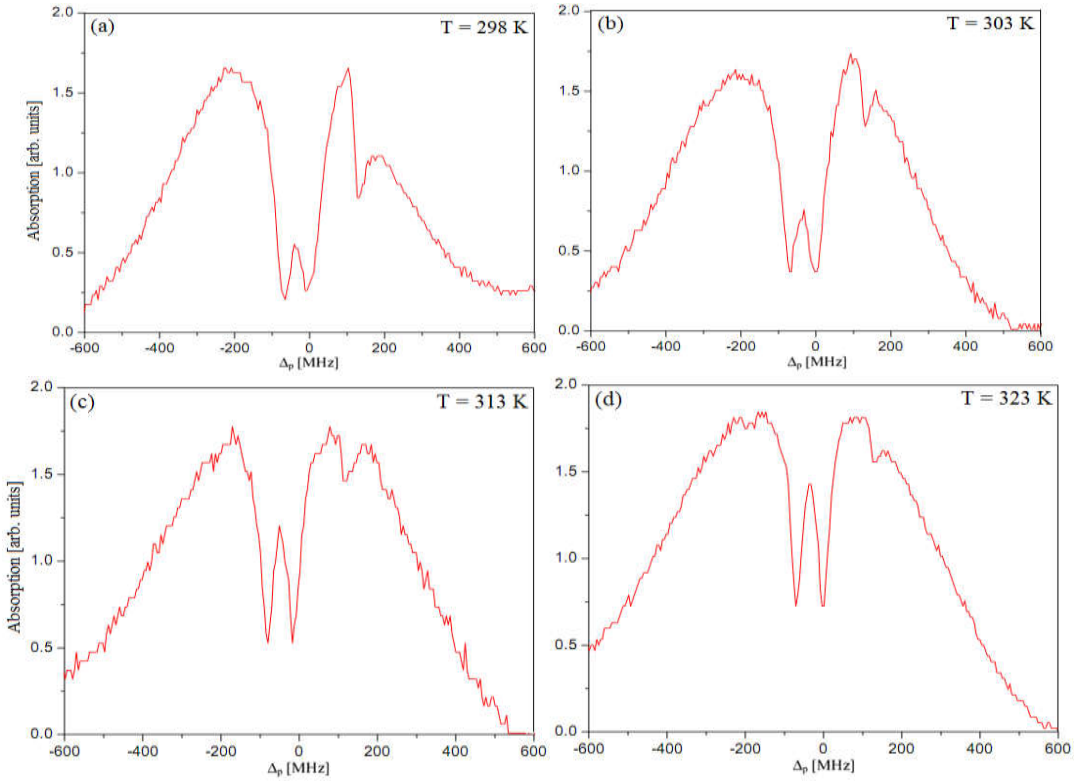

Fig. 11. Experimental absorption spectrum of atomic medium measured at Ω_c = 240 MHz and Δ_c = 0 for various temperatures, 298 K (a), 303 K(b), 313 K (c), and 323 K (d) [76].

IV. GIANT KERR NONLINEARITY

In the past decades, we have witnessed a tremendous progress of study related to EIT enhanced Kerr nonlinearity because it concerns several interesting and potential applications, such as cross-phase modulation for optical shutters [23], self-phase modulation for generating optical solitons [85], four-wave mixing processes for frequency conversion [86], and entangled states for quantum information processing [87]. Firstly, Schmidt *et al* [23] theoretically demonstrated that cross-Kerr nonlinearity is enhanced significantly in the presence of the EIT effect and then is experimentally demonstrated by Kang [24]. Wang *et al.* [25], for the first time performed a direct measurement of self-Kerr coefficient in a three-level lambda EIT medium by using the ring cavity scanning technique. The measurement shows a great enhancement of the Kerr nonlinear index of refraction in several orders of magnitude around atomic resonance. Theoretically, in a recent work [26] we have built an analytical model to represent self-Kerr nonlinear spectra of three-level lambda-type system. So far, enhancement of Kerr nonlinearity in multi-level system has been proposed extensively. Particularly, multi-level systems were proposed to enhance cross-Kerr [88, 89] and self-Kerr [59-61] nonlinearity. Recently, Bang and co-workers [77] have developed an

analytical model to study the enhancement and control of self-Kerr nonlinearity in the five-level atomic medium.

The expression of Kerr nonlinear coefficient can be obtained by solving Eq. (1) for the matrix element ρ_{21} up to the third order under the perturbation theory. The third-order susceptibility is, thus, given by [77]

$$\chi^{(3)} = -\frac{Nd_{21}^4}{3\varepsilon_0\hbar^3}\frac{1}{\Gamma_{21}}\frac{B}{A^2+B^2}\left(\frac{A}{A^2+B^2}+i\frac{B}{A^2+B^2}\right), \tag{29}$$

where A and B are controllable parameters given by Eqs. (10) and (11).

Having the third-order nonlinear susceptibility, the Kerr nonlinear coefficient n_2 for the probe light was derived as [77]

$$n_2 = \frac{12\pi^2 Re(\chi^{(3)})}{n_0^2 c} = -\frac{4\pi^2 Nd_{21}^4}{\varepsilon_0\hbar^3 c}\frac{1}{\Gamma_{21}}\frac{AB}{\left(1+4\pi\frac{Nd_{21}^2}{\varepsilon_0\hbar}\frac{A}{A^2+B^2}\right)(A^2+B^2)^2}. \tag{30}$$

The expression (30) represents the self-Kerr nonlinear coefficient for the probe light as a function of intensity and frequency detuning of the coupling light. The influence of EIT on Kerr nonlinearity is shown in Fig. 12 by comparing value of n_2 between the cases of presence and absence of EIT effect. It is apparent to see a basic modification and great enhancement of the self-Kerr nonlinear coefficient in the five-level system under the presence of EIT.

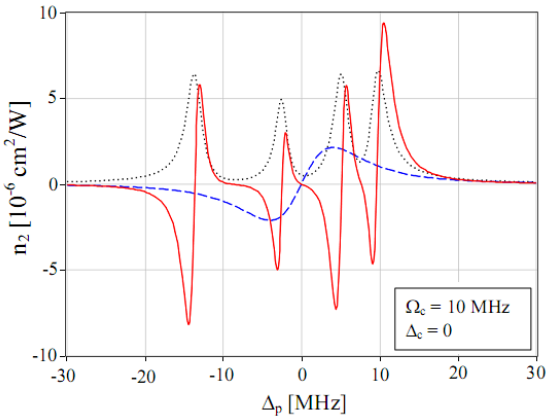

Fig. 12. Variation of the Kerr coefficient n_2 with the respect to probe frequency detuning in the cases of the five-level cascade system (solid line) and in the two-level system (dashed line), at zero frequency detuning of the coupling light. The dotted line stands for EIT spectrum [77].

The modification of Kerr nonlinearity of the five-level system is due to quantum interference effect between transition channels among the states. Furthermore, in each spectral region corresponding to an EIT transparent window (represented by the dotted line in Fig. 12), there is pair of positive-negative peaks of n_2. An important feature is that one may control peaks and slops of the Kerr coefficient to vary from positive to negative, and versa, by tuning frequency of the coupling light. For example, the negative peak of n_2 (positioned in the spectral region of the center

EIT transparent window in Fig. 12) corresponding to Δ_p = 4.5 MHz can be changed to a positive peak, as in Fig. 13. The change of the negative peak of n_2 into positive peak at certain values of probe frequency shows a feasible way to control amplitude, sign, and slop of Kerr coefficient.

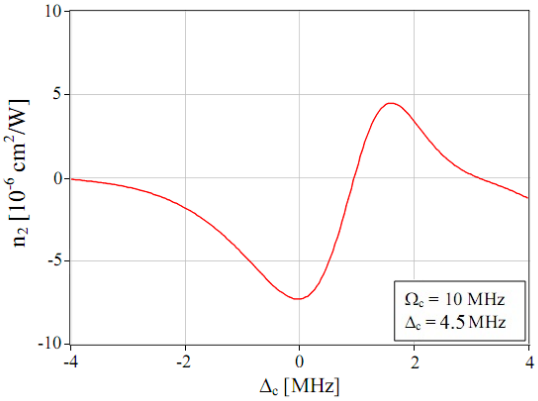

Fig. 13. Variations of n_2 when $\Omega_c = 10$ MHz and $\Delta_p = 4.5$ MHz [77].

The influence of the coupling light intensity on Kerr nonlinearity is shown in Fig. 14, where $\Delta_p = 4.5$ MHz and $\Delta_c = 0$, that corresponding to the negative peak in the spectral region of the center EIT transparent window in Fig. 12.

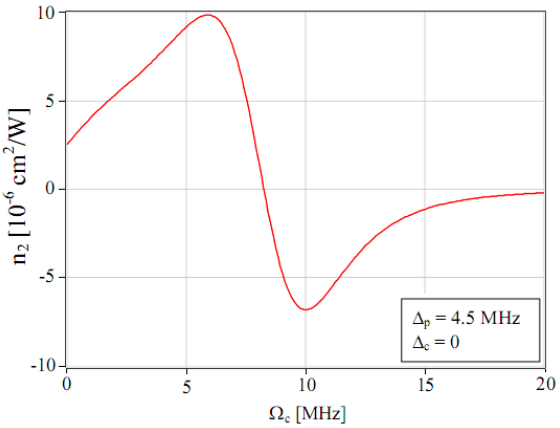

Fig. 14. Variations of n_2 with the respect to coupling light intensity at fixed values of frequency detuning of the probe (Δ_p = 4.5 MHz) and coupling (Δ_c = 0) lights [77].

For the case of the Doppler broadening, the third-order nonlinear susceptibility is modified to [26]

$$\chi^{(3)}(v)dv = -\frac{iN_0 d_{21}^4}{3u\sqrt{\pi}\varepsilon_0\hbar^3}\left(\frac{1}{2\gamma+\gamma_{21}}\right)\frac{e^{-v^2/u^2}}{F(v)}\left[\frac{1}{F(v)}+\frac{1}{F^*(v)}\right]dv, \tag{31}$$

where $u = \sqrt{2k_BT/m}$, and

$$F(v) = \gamma - i\left(\Delta_p + \frac{v}{c}\omega_p\right) + \frac{\Omega_c^2/4}{\gamma_{31} - i(\Delta_p - \Delta_c) - i\frac{v}{c}(\omega_p - \omega_c)}. \tag{32}$$

Since $\omega_p$is close to ω_c so term $i\frac{v}{c}(\omega_p - \omega_c)$ in (32) can be neglected. The third-order nonlinear susceptibility is calculated by integrating Eq. (31) over the velocity distribution [26]:

$$\chi^{(3)} = -\frac{iN_0 d_{21}^4}{3\sqrt{\pi}\varepsilon_0\hbar^3(\omega_p u/c)^2}\left(\frac{1}{2\gamma+\gamma_{21}}\right)$$

$$\times\left\{2\sqrt{\pi}\left(-1+\sqrt{\pi}ze^{z^2}[1-erf(z)]\right)+\frac{\pi\left(e^{z^2}[1-erf(z)]+e^{z^{*2}}[1-erf(z^*)]\right)}{z+z^*}\right\}, \tag{33}$$

where

$$z = \frac{c}{\omega_p u}\left(\gamma - i\Delta_p + \frac{\Omega_c^2/4}{\gamma_{31} - i(\Delta_p - \Delta_c)}\right) = \frac{c}{\omega_p u}F, \tag{34}$$

with z^* presenting the complex conjugation of z, and *erf* is error function.

Having the linear and third-order nonlinear susceptibilities, the nonlinear Kerr index of refraction n_2 is determined with Eq. (30).

Fig. 15a shows variation of the Kerr nonlinear coefficient n_2 versus the probe frequency detuning. It is apparent to see a fundamental modification and a great enhancement of the self-Kerr nonlinear coefficient in the three-level system under the present of the EIT effect. Such behavior of the obtained analytical result is tested by comparing with experimental observation in Ref. [25] as shown in Fig. 15b. The comparison confirms a good agreement between the theoretical calculation and measurement.

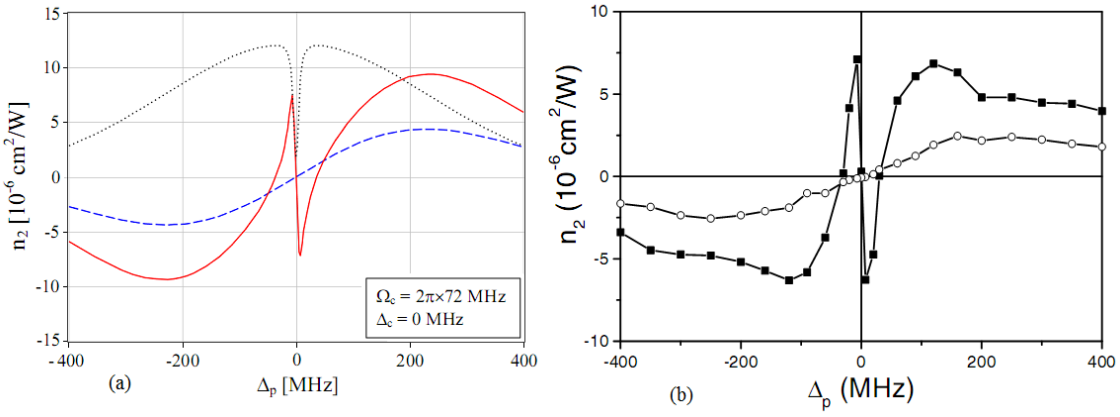

Fig. 15. (a) – Theoretical plots of Kerr nonlinearity n_2 versus probe detuning Δ_p for the present (dashed curve) and absent (solid curve) of the EIT effect at temperature 336 K and $\Delta_c = 0$[26]. (b) - Experimental measurement of n_2 in the Ref. [25] for $\Delta_c = 0$ and $\Omega_c = 2\pi\times72$ MHz, where the square- and circular- curves stand for the present and absent of the coupling light, respectively.

The influence of frequency of the coupling light on the Kerr nonlinear coefficient is considered by investigating the variation of n_2 with respect to frequency detuning Δ_c. The authors in Ref. [26] chose a zero value of n_2 corresponding to $\Delta_p = 0$ and $\Omega_c = 2\pi\times72$ MHz as in Fig. 15a. Variation of the Kerr coefficient versus frequency of the coupling light is shown in Fig. 16a. It shows changes in both magnitude and sign of the Kerr nonlinear coefficient.

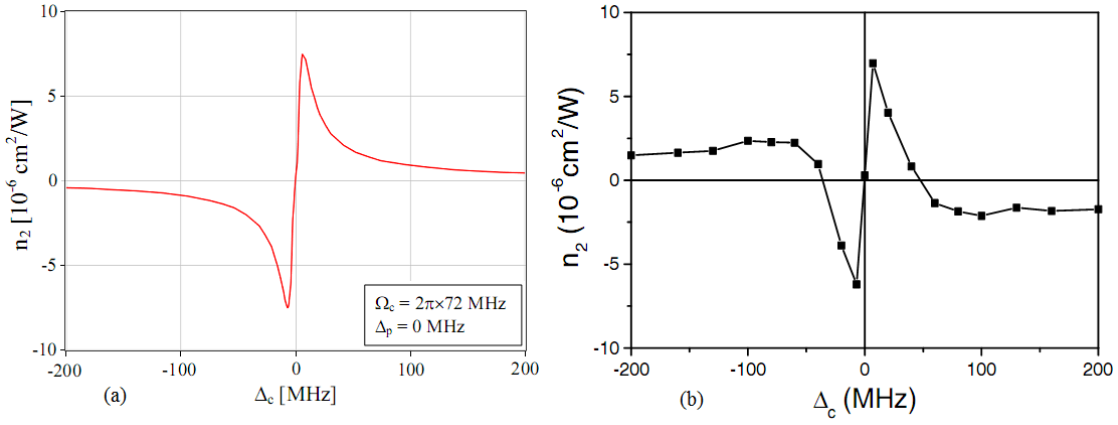

Fig. 16. Variation of magnitude and sign of the Kerr nonlinear coefficient n_2 versus frequency detuning of the coupling field when $\Delta_p = 0$ and $\Omega_c = 2\pi \times 72$ MHz. Figures (a) and (b) represent theoretical calculation [26] experimental measurement [25], respectively.

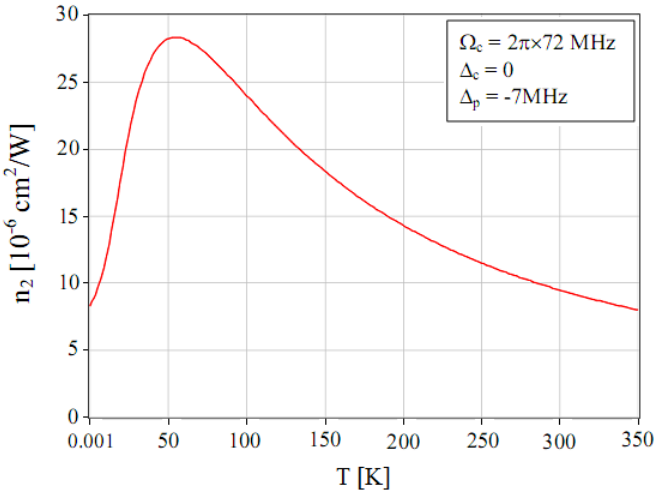

Fig. 17. Variation of the Kerr nonlinear coefficient versus absolute temperature when $\Delta_p = -7$ MHz, $\Delta_p = 0$, and $\Omega_c = 2\pi \times 72$ MHz [26].

The influence of temperature on magnitude of the Kerr coefficient is shown in Fig. 17, where the authors in [26] chose the maximum point of n_2 corresponding to parameters $\Delta_c = 0$, Δ_p

= -7 MHz, and Ω_c = $2\pi\times$72 MHz, as indicated by the solid line in Fig. 15a. It shows that, for a given set of fixed values of the parameters Δ_c, Δ_p, and Ω_c it could be able to choose an optimized temperature to have largest value of the self-Kerr coefficient n_2. For the parameters indicated in Fig. 17, the expected temperature for largest value of n_2 is estimated about 57 K [26].

V. CONTROLLING GROUP VELOCITY OF MULTI-FREQUENCY LIGHT

Along with zero absorption in the vicinity of resonant frequency, on dispersion profile appears a normal dispersive curve with its height and slope being controllable by the coupling laser field. Therefore, the dispersion $dn/d\omega$ becomes very large in EIT window. This is the basis to control group velocity of light.

Slow (subluminal) and fast (superluminal) lights have potential impact on photonic technology which have opened up several fascinating applications, as controllable optical delay lines, optical switching, telecommunication, interferometry, optical data storage and optical memories, and quantum information processing [90-93]. In general, subluminal propagation takes place at the normal dispersive regions, while superluminal propagation normally corresponds to abnormal dispersive regions in a dispersive medium. The key to manipulate light speed is controllable dispersive properties of a medium under laser fields. Indeed, magnitude and sign of dispersion of the medium for a probe light field is controlled by another coupling light field based on EIT technique. Several researchers attempted to demonstrate experimentally in subluminal [31, 32, 94-97] and superluminal [98-101] lights. Recently, studies have also been done on the switching between the subluminal and superluminal propagations in an atomic medium by changing frequency, intensity, phase and polarization of applied fields [57, 58, 102-110]. Moreover, some research groups used multiple EIT to control the group velocity at multiple frequencies [42, 46, 56-58]. Bang and coworkers have developed an analytical model to study the control of group velocity in the five-level cascade atomic medium under Doppler broadening [80] and self-Kerr nonlinearity [81].

The group index and group velocity of the probe field can be written as [81]

$$n_g = n + \omega_p \frac{\partial n}{\partial \omega_p}, \tag{35}$$

$$v_g = \frac{c}{n_g}. \tag{36}$$

In the case of absence of Doppler broadening, the linear index n and the group index n_g are determined by [80],

$$n = 1 + \frac{Nd_{21}^2}{2\varepsilon_0\hbar}\frac{A}{A^2+B^2}, \tag{37}$$

$$n_g \simeq \omega_p \frac{Nd_{21}^2}{2\varepsilon_0\hbar}\left[\frac{A'(A^2+B^2)-2A(AA'+BB')}{(A^2+B^2)^2}\right], \tag{38}$$

where $A\prime$ and $B\prime$ represent the derivatives of A and B over ω_p, respectively, which are given by:

$$\begin{aligned} A' = &-1 + \frac{A_{32}}{\gamma_{31}(\Delta_p+\Delta_c)} - \frac{2A_{32}^2}{a_{32}^2(\Omega_c/2)^2\gamma_{31}^2} + \frac{A_{42}}{\gamma_{41}(\Delta_p+\Delta_c+\delta_1)} - \frac{2A_{42}^2}{a_{42}^2(\Omega_c/2)^2\gamma_{41}^2} \\ &+ \frac{A_{52}}{\gamma_{51}(\Delta_p+\Delta_c-\delta_2)} - \frac{2A_{52}^2}{a_{52}^2(\Omega_c/2)^2\gamma_{51}^2}, \end{aligned} \tag{39}$$

$$B' = -\frac{2A_{32}^2}{a_{32}^2(\Omega_c/2)^2\gamma_{31}(\Delta_p+\Delta_c)} - \frac{2A_{42}^2}{a_{42}^2(\Omega_c/2)^2\gamma_{41}(\Delta_p+\Delta_c+\delta_1)} - \frac{2A_{52}^2}{a_{52}^2(\Omega_c/2)^2\gamma_{51}(\Delta_p+\Delta_c-\delta_2)}. \tag{40}$$

On the other hand, it is noted that, the EIT windows appear at two-photon resonance conditions, namely, $\Delta_p + \Delta_c = 0$, $\Delta_p + \Delta_c + \delta_1 = 0$ and $\Delta_p + \Delta_c - \delta_2 = 0$. Therefore, the group index in each EIT window can be approximated by [81]:

$$n_{g32}\Big|_{\substack{\Delta_c=0\\ \Delta_p=0}} = \frac{2\omega_p N d_{21}^2}{\varepsilon_0\hbar}\frac{a_{32}^2\Omega_c^2 - 4\gamma_{31}^2}{\left(a_{32}^2\Omega_c^2 + 4\gamma_{21}\gamma_{31}\right)^2}, \tag{41}$$

$$n_{g42}\Big|_{\substack{\Delta_c=0\\ \Delta_p=-\delta_1}} = \frac{2\omega_p N d_{21}^2}{\varepsilon_0\hbar}\frac{\left(a_{42}^2\Omega_c^2 - 4\gamma_{41}^2\right)\left[\left(a_{42}^2\Omega_c^2 + 4\gamma_{21}\gamma_{41}\right)^2 - \left(4\delta_1\gamma_{41}\right)^2\right]}{\left[\left(4\delta_1\gamma_{41}\right)^2 + \left(a_{42}^2\Omega_c^2 + 4\gamma_{21}\gamma_{41}\right)^2\right]^2}, \tag{42}$$

$$n_{g52}\Big|_{\substack{\Delta_c=0\\ \Delta_p=\delta_2}} = \frac{2\omega_p N d_{21}^2}{\varepsilon_0\hbar}\frac{\left(a_{52}^2\Omega_c^2 - 4\gamma_{51}^2\right)\left[\left(a_{52}^2\Omega_c^2 + 4\gamma_{21}\gamma_{51}\right)^2 - \left(4\delta_2\gamma_{51}\right)^2\right]}{\left[\left(4\delta_2\gamma_{51}\right)^2 + \left(a_{52}^2\Omega_c^2 + 4\gamma_{21}\gamma_{51}\right)^2\right]^2}. \tag{43}$$

The appearance of regions corresponding to slow or fast light at multi-frequency is plotted in Fig. 18. Here, the values of the coupling laser was chosen as Δ_c = 0 and Ω_c = 4 MHz. It shows three frequency regions of the probe light (centered at Δ_p = -9 MHz, Δ_p = 0, and Δ_p = 7.6 MHz) each of which behavior positive and negative group index, or subluminal and superluminal propagation, respectively.

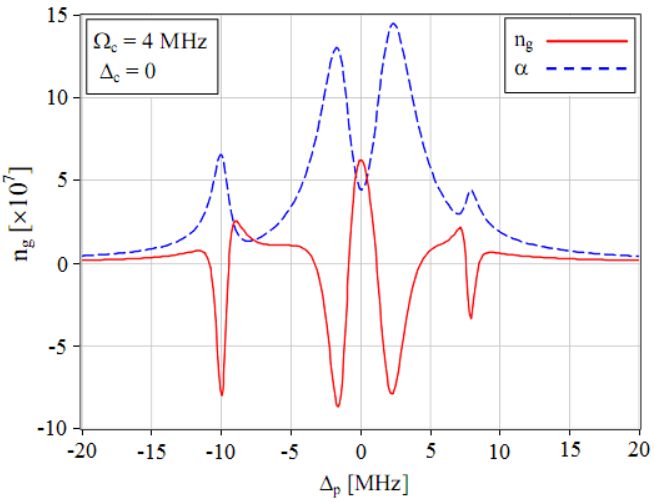

Fig. 18. Variation of the group index versus probe frequency detuning when $\Omega_c = 4$ MHz and $\Delta_c = 0$. The dotted line represents EIT spectrum [81].

Fig. 19 is plot of the group index n_g versus the coupling Rabi frequency (intensity) Ω_c at the fixed values Δ_c = 0 and Δ_p = 0 (solid line), Δ_p = -9 MHz (dashed line), and Δ_p = 7.6 MHz

(dotted line) that corresponds to the center of each EIT window. It is shown that the group index is varied between negative and positive values at the three frequency regions. As a consequence, the probe light propagation can be manipulated between the superluminal and subluminal modes by tuning the coupling intensity.

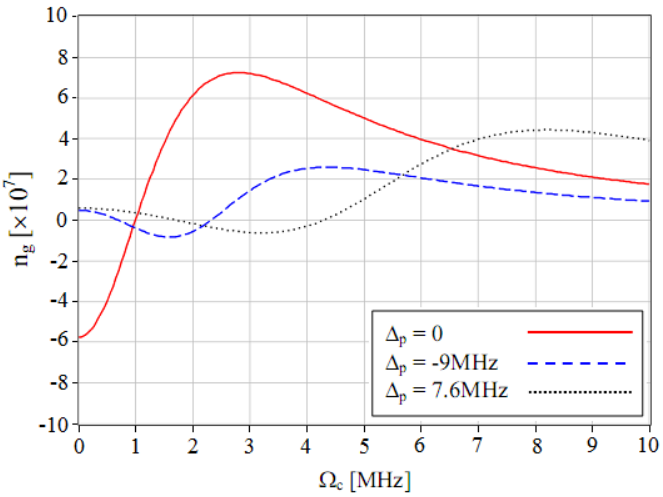

Fig. 19. Plots of n_g versus Ω_c when $\Delta_c = 0$ and $\Delta_p = 0$ (solid line), Δ_p = -9 MHz (dashed line), and $\Delta_p = 7.6$ MHz (dotted line) [81].

From analytical point of view, using Eq. (41) a minimum value of the group velocity can be found at the following Rabi frequency:

$$\Omega_c = 2\sqrt{(\gamma_{21}+2\gamma_{31})\gamma_{31}}. \tag{44}$$

At such Rabi frequency, the minimum group velocity in the first EIT window is determined as,

$$\left(v_{g32}^{(0)}\right)_{\min} = \frac{8\varepsilon_0\hbar c}{\omega_p N d_{21}^2}(\gamma_{21}+\gamma_{31})\gamma_{31}. \tag{45}$$

It is shown from Eq. (45) that the group velocity depends on the damping rate γ_{31} or depends inversely on life-times of the excited electronic states. For the excited states having a life-time of few *ns*, the minimum group velocity can be few m/s. However, the cascade excitation scheme can deliver a possible way to choose the uppermost excited states as the Rydberg states which have life-time of few μs. In this case, one may slow down the probe light to few *mm/s* (ultraslow light). On the other hand, Eq. (45) shows that one may further slowdown the probe light by increasing atomic density.

In Fig. 20 the authors in [81] showed variation of the group indices n_g versus the coupling frequency when the probe field frequency is resonant with the transition $|1\rangle \leftrightarrow |2\rangle$, i.e., Δ_p= 0 and Ω_c = 4 MHz. The group velocity of the probe field can be switched between the subluminal and superluminal regime by tuning the coupling laser frequency.

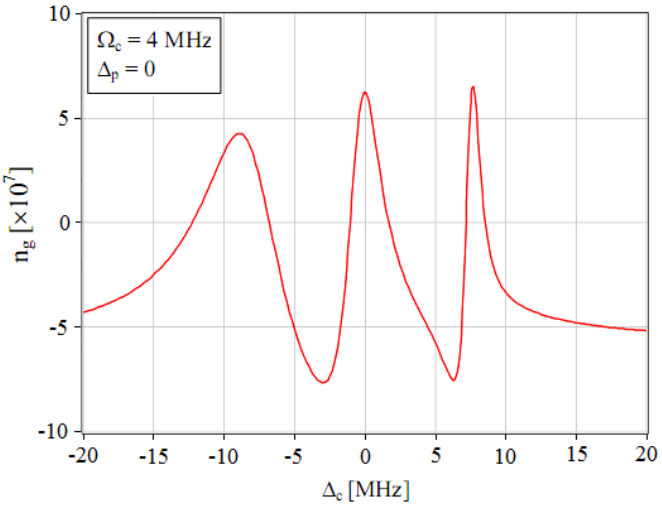

Fig. 20. Variation of group index versus coupling frequency detuning when $\Delta_p = 0$ and $\Omega_c = 4$ MHz [81].

For a vapor medium, it is necessary to consider the Doppler effect on the susceptibility. The group index for the probe field in the case of Doppler broadening can be written as

$$n_g^{(D)} = n + \omega_p \frac{\partial n}{\partial \omega_p}, \tag{46}$$

where n is dispersion coefficient that is determined by the real part of the linear susceptibility, Eq. (27). The group velocity and the group index are related as

$$v_g^{(D)} = \frac{c}{n_g^{(D)}}. \tag{47}$$

The plot of the group index versus the probe frequency detuning for the cases of absence (dashed line) and presence (solid line) of Doppler broadening (corresponding to room temperature 300 K) is shown in Fig. 21. As pointed out in [80] the maximum group index can occur at the transparency efficiency about 50%, therefore to compare the group velocity in both cases the authors used value of Ω_c which corresponds to transparent efficiency of 50% for each case. Fig. 21(a) shows variation of transparent efficiency R_{32} with the respect to Ω_c. It is shown that the transparent efficiency approaches to 50% when $\Omega_c = 2.5$ MHz or $\Omega_c = 22$ MHz which correspond to the absence or presence of Doppler effect (at $T = 300$ K), respectively.

As shown in Fig. 21(b), there are three frequency regions of the probe light (centered at $\Delta_p = -9$ MHz, $\Delta_p = 0$, and $\Delta_p = 7.6$ MHz), each of which has positive and negative group index, or subluminal and superluminal propagation mode, respectively. On the other hand, Doppler broadening leads to decrease of the group index or increase of the group velocity by few orders compared to the case when Doppler effect is absent. For example, at $\Delta_p = 0$ as in Fig. 21(b), $n_g^{(0)} \sim 5.6 \times 10^5$ (or group velocity $v_g^{(0)} \sim 5.3 \times 10^2$ m/s), while $n_g^{(0)} \sim 1.2 \times 10^3$ (or group velocity $v_g^{(D)} \sim 2.5 \times 10^5$ m/s). In order to further consider influence of Doppler effect, the authors in Ref.

[80] plotted group index versus the temperature at a fixed value $\Omega_c = 22$ MHz, that corresponds to 50% of the R_{32}, as displayed in Fig. 22. It is shown that as the temperature increases the magnitude of group index decreases gradually.

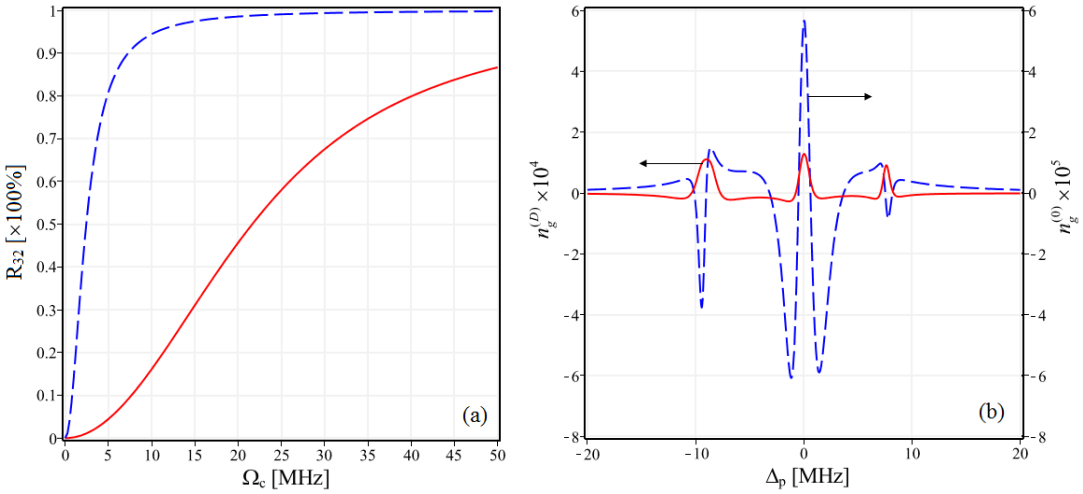

Fig. 21. Plot of transparent efficiency R_{32} (a) and group index (b) for the cases of the Doppler broadening absented (dashed line) and presented (solid line) when Δ_c = 0; In the Fig. (b), the value of Ω_c is chosen as 2.5 MHz for the absence and 22 MHz for the presence of Doppler broadening, respectively [80].

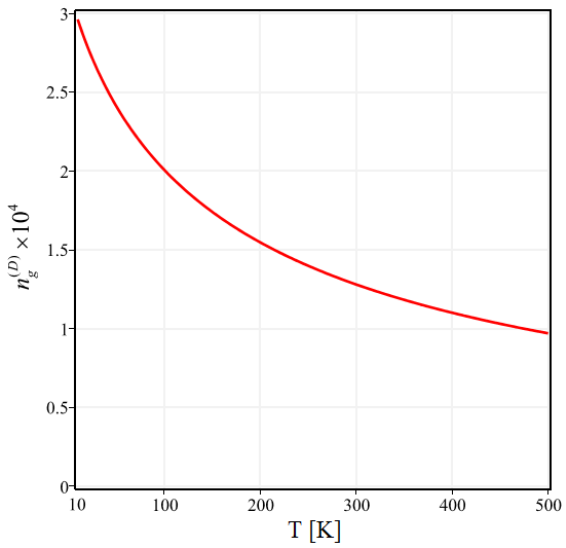

Fig. 22. Variation of group index $n_g^{(D)}$ versus the temperature at $\Delta_p = \Delta_c$ = 0 and $\Omega_c = 22$ MHz [80].

The location of subluminal and superluminal regions can be controlled by the coupling field's frequency as illustrated in Fig. 23, where group index $n_g^{(D)}$ is plotted at different values Δ_c = -5 MHz, Δ_c = 0, and $\Delta_c = 5$ MHz. It is shown in Fig. 23(a) that one may shift systematically the subluminal and superluminal regions to the red or blue directions when the coupling frequency is tuned to the blue or red side, respectively. On the other hand, the subluminal light can be switched between the superluminal and subluminal mode by tuning frequency of the coupling field.

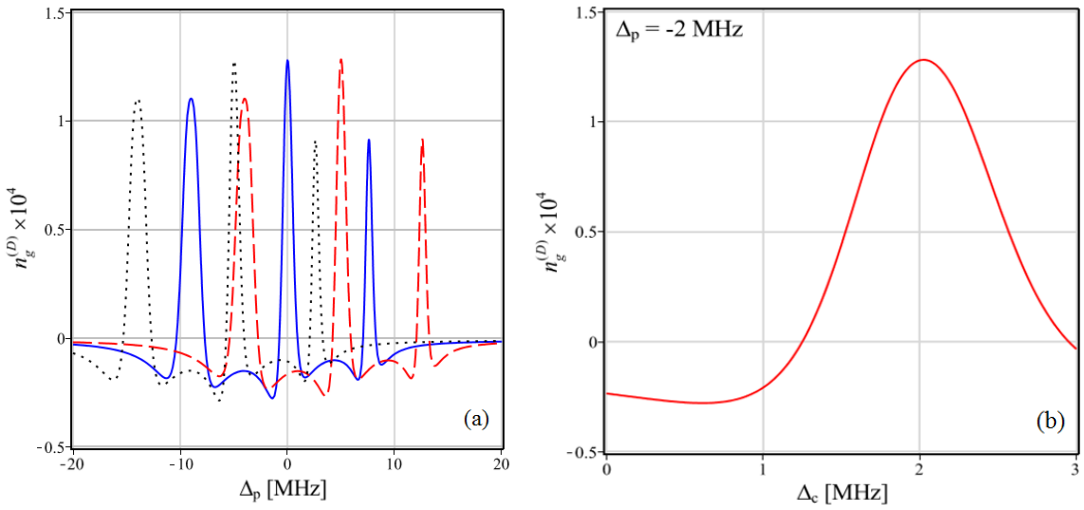

Fig. 23. (a) - Systematic shift of the subluminal and superluminal regions when tuning frequency of the coupling field to $\Delta_c = -5$ MHz (*dashed*), Δ_c = 0 (*solid*), and Δ_c = 5 MHz (*dotted*); (b) - Variation of the group index $n_g^{(D)}$ versus Δ_c when Δ_p = -2 MHz. Both cases are plotted at Ω_c = 22 MHz and $T = 300$ K [80].

In Fig. 24, the group index $n_g^{(D)}$ (solid line) is plotted at $\Delta_p = 2$ MHz, $\Delta_c = 0$ and $T = 300$ K. It shows that the group index is varied between negative and positive values under variation of the coupling intensity. As a consequence, the probe light propagation can be manipulated between the superluminal- and subluminal-mode. Indeed, tuning range of Ω_c to switch from a negative peak to a nearby positive peak of the group index is about $\Delta\Omega_c = 4$ MHz or $\Delta\Omega_c = 30$ MHz for the absence or presence of Doppler broadening, respectively (Fig. 24). This difference can be explained with a notice that the Doppler broadening makes absorption profile broader thus enlarges distance between two adjacent positive and negative peaks of the group index.

As pointed out in Sec. IV, an interesting property of the EIT medium is exhibition of giant Kerr nonlinearity with its controllable magnitude and sign [77]. As a consequence, such a nonlinearity influences on the group velocity of light in the EIT media, even at very low light intensity. Indeed, Agarwal *et al.* [111] demonstrated that cross-Kerr nonlinearity makes a significant contribution to the group velocity. More recently, Ali *et al.* [112] showed that the light could be further slowed by the cross-Kerr nonlinearity. In addition to the cross-Kerr, giant self-Kerr nonlinearity also arises in the EIT medium [23]. In the presence of the self-Kerr nonlinearity, the group index

under the presence of self-Kerr nonlinearity can therefore be determined as [113]:

$$n_g^{(K)} = n + \omega_p \frac{\partial n}{\partial \omega_p} = n_0 + n_2 I_p + \omega_p \left(\frac{\partial n_0}{\partial \omega_p} + \frac{\partial n_2}{\partial \omega_p} I_p \right). \tag{48}$$

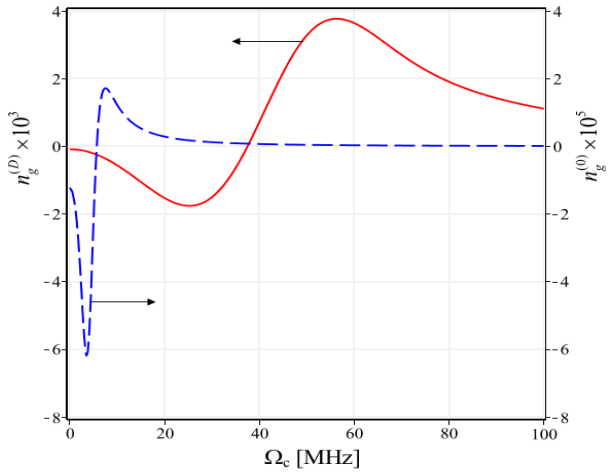

Fig. 24. Plots of $n_g^{(0)}$ (dashed line) and $n_g^{(D)}$ (solid line) when $\Delta_p = 2$ MHz, $\Delta_c = 0$, and $T = 300$ K [80].

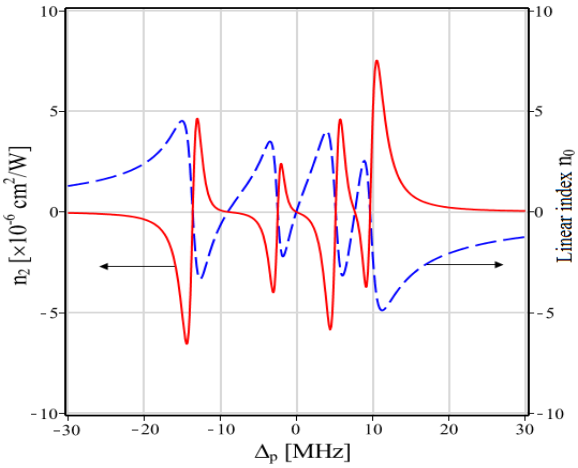

Fig. 25. Variations of the self-Kerr nonlinearity n_2 (*solid*) and linear index of refraction n_0 (*dashed*) versus the probe frequency detuning Δ_p when Ω_c = 10 MHz and Δ_c = 0 [81].

Figure 25 shows variations of linear and nonlinear indices versus the probe frequency detuning Δ_p for the fixed parameters Ω_c = 10 MHz and Δ_c = 0. We can see a normal and anomalous dispersion of the linear index (*dashed curve*) in three separated regions corresponding to three EIT windows which center at Δ_p = -9 MHz, Δ_p = 0, and Δ_p = 7.6 MHz. Such dispersive property

delivers both sub- and super-luminal propagation modes for the multi-frequency probe light. On the other hand, the dispersion of the linear index is opposite direction with that of the self-Kerr nonlinearity (*solid curve* in Fig. 25), thus the giant self-Kerr nonlinearity can reduce the effective index or enhance the group velocity of the probe light (see Fig. 26a). Furthermore, the self-Kerr nonlinearity leads to variation of both magnitude and sign of the group index under changing probe intensity, frequency consequently, one that may manipulate the probe light propagation to propagate between sub- and supper- luminal modes by tuning its own intensity (Fig. 26b). This variation can be explained from Eq. (48) that the group index depends proportionally on intensity of the probe light, thus influence of the self-Kerr nonlinearity is more efficient with high intensity of the probe light.

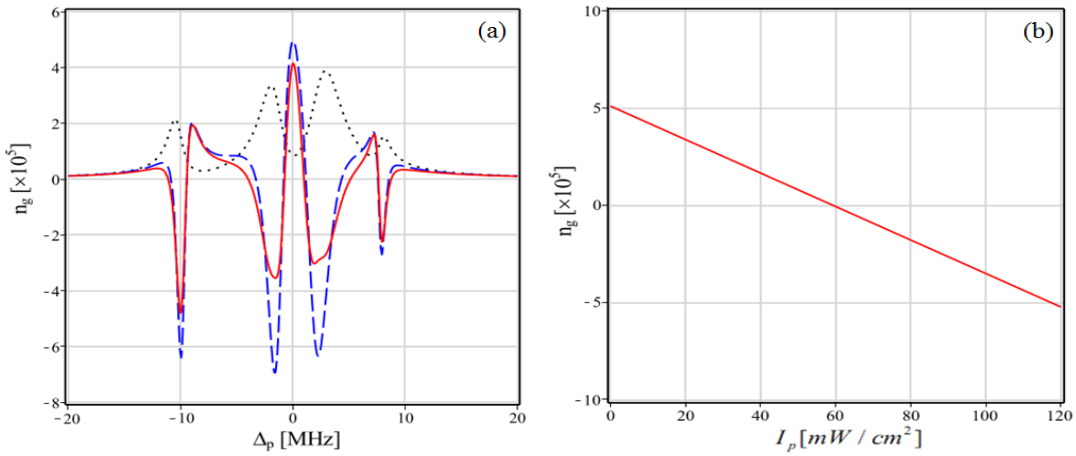

Fig. 26. (a) - variation of the group index in the present (*solid*) absent (*dashed*) of self-Kerr nonlinearity when I_p =10 mW/cm^2, $\Omega_c = 4$ MHz and $\Delta_c = 0$; the dotted curve represents EIT spectrum. (b) - variation of the Kerr nonlinearity $n_g^{(K)}$ versus probe intensityI_p when $\Omega_c = 4$ MHz and $\Delta_c = \Delta_p = 0$ [81].

VI. CONTROLLING OPTICAL BISTABILITY

The optical bistability (OB) is one of the most interesting fields of research in nonlinear optics because it has a large number of potential applications in both optical sciences and photonics technology, as all-optical switches, all-optical memories, optical transistors, and all-optical logic gates and processors [114]. In the early years of the OB research for atomic media, a great interest was focused to the two-level atomic system [115]. The saturated absorption and intensity-dependent refractive index of the media are attributed to two different mechanisms for the absorptive OB and dispersive OB, respectively. It was shown that, bistable states occur only in certain values of input intensity [115]. Although, the usual OB behaviors of the two-level atomic system were observed experimentally but there is still lack of applications due to only one optical field being employed for both applying and switching, thus lack of control for switching intensity thresholds.

In recent years, the OB in EIT media has been extensively studied. Due to the controllable optical properties, both switching intensity thresholds and width of the OB can be simply controlled by either intensity or relative phase of applied field [116-122]. Indeed, OB in the multi-level systems has also been studied extensively, e.g., four-level EIT configurations with two controlling fields [123-127], and a Kobrak - Rice 5-level system [128] with four controlling fields. More recently, the OB model consisting of a five-level cascade EIT medium placed inside a ring cavity has been proposed [78]. We assume a medium of length L composed of Nfive-level cascade systems placed in a unidirectional ring cavity as shown in Fig. 27.

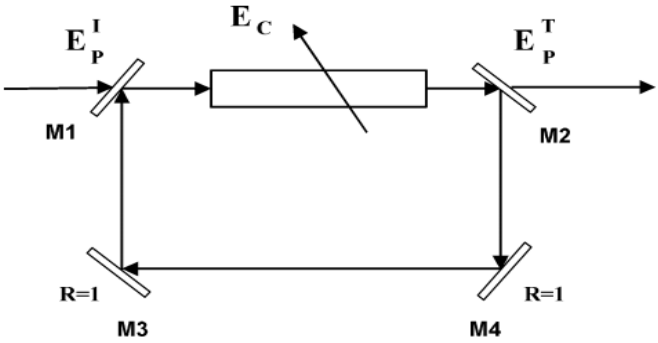

Fig. 27. The schematic setup of an indirectional ring cavity: E_p^I and E_p^T denote the incident and transmitted probe field, respectively; E_c represents the coupling field that is not circulated inside the cavity [28].

For simplicity, we assume both mirrors M3 and M4 are perfect reflective whereas both mirrors M1 and M2 are the same, each has a reflectivity R and transmittivity T, with $R+T=1$. In the ring cavity configuration, the probe field E_p is circulated in the ring cavity but nor the coupling field E_c. By normalizing the incident and transmitted probe field by

$$Y=\frac{d_{21}E_p^I}{\hbar\sqrt{T}},\quad X=\frac{d_{21}E_p^T}{\hbar\sqrt{T}}, \tag{49}$$

the input-output relationship for the probe field under the slowly varying envelop approximation is given as [78]:

$$Y=X-\frac{CX}{2}\frac{(\tilde{\gamma}_{21}^*+F_1^*+F_2)}{F_1F_1^*-(\tilde{\gamma}_{21}^*+F_2)(\tilde{\gamma}_{21}+F_2^*)}, \tag{50}$$

where

$$C=\frac{N\omega_pLd_{21}^2}{2c\varepsilon_0\hbar T}, \tag{51}$$

is the cooperation parameter of the five-level system placed in the ring cavity,

$$F_1=\frac{\Omega_c}{2}\left(\frac{a_{32}A_1}{A}+\frac{a_{42}B_1}{B}+\frac{a_{52}D_1}{D}\right), \tag{52}$$

$$F_2=\frac{\Omega_c}{2}\left(\frac{a_{32}A_2}{A}+\frac{a_{42}B_2}{B}+\frac{a_{52}D_2}{D}\right), \tag{53}$$

$$\tilde{\gamma}_{21} = i\Delta_p - \gamma_{21}, \tag{54}$$
$$\tilde{\gamma}_{31} = i(\Delta_p + \Delta_c) - \gamma_{31}, \tag{55}$$
$$\tilde{\gamma}_{41} = i(\Delta_p + \Delta_c + \delta_1) - \gamma_{41}, \tag{56}$$
$$\tilde{\gamma}_{51} = i(\Delta_p + \Delta_c - \delta_2) - \gamma_{51}, \tag{57}$$
$$\tilde{\gamma}_{32} = i\Delta_c - \gamma_{32}, \tag{58}$$
$$\tilde{\gamma}_{42} = i(\Delta_c + \delta_1) - \gamma_{42}, \tag{59}$$
$$\tilde{\gamma}_{52} = i(\Delta_c - \delta_2) - \gamma_{52}. \tag{60}$$

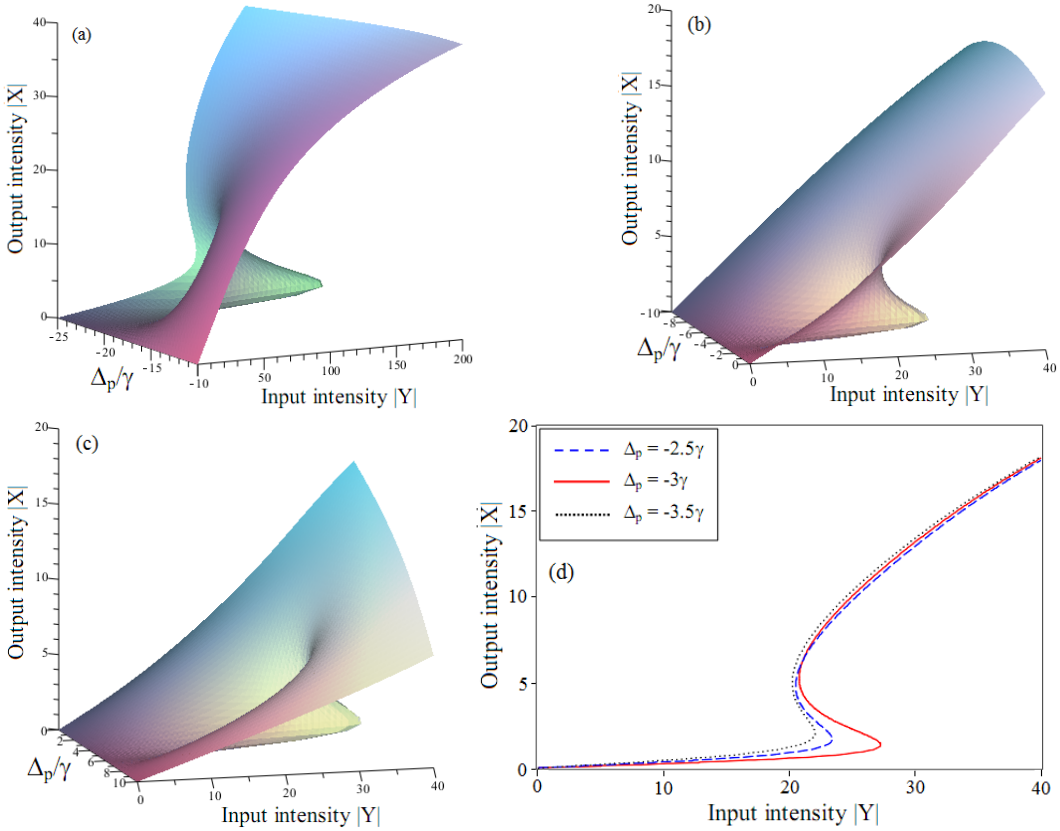

Fig. 28. (a)-(c) Surface plots of OB for the probe field at $\Omega_c = 20\gamma, \Delta_c = 0$, and $C = 1000\gamma$. Three separated spectral regions of OB corresponding to the coupling transitions between the states $|2\rangle \leftrightarrow |4\rangle$, $|2\rangle \leftrightarrow |3\rangle$, and $|2\rangle \leftrightarrow |5\rangle$, respectively; (d) OB hysteresis loops at different values of the frequency detuning [78].

A surface plot of OB in a region of the probe detuning from -25 MHz to 10 MHz is shown in Fig. 28. It is easy to see an OB behavior in three separated regions. Such simultaneous occurrence of OB at a certain value of input intensity in three spectral regions is completely different from

that of the three and four level systems [78]. On the other hand, in each window, the OB hysteresis loop is changed with variations of frequency of the probe field. For a detail, the authors in Ref. [78] plotted the input-output intensity relationship at specific values of the frequency detuning, as shown in Fig.28(d).

The influence of intensity and frequency detuning of the coupling light on OB hysteresis loop is shown in Fig. 29. It is shown that the switching thresholds can be changed by tuning the intensity and/or the frequency detuning of the coupling light. The physics to explain the case in Fig. 29 (a) is due to a sensitive dependence of Kerr nonlinearity on the coupling frequency whereas the case in Fig. 29(b) comes from the growing of Kerr nonlinearity under increasing the coupling intensity Ω_c in the plotted region, as shown in Fig. 12, thus reduces switching thresholds.

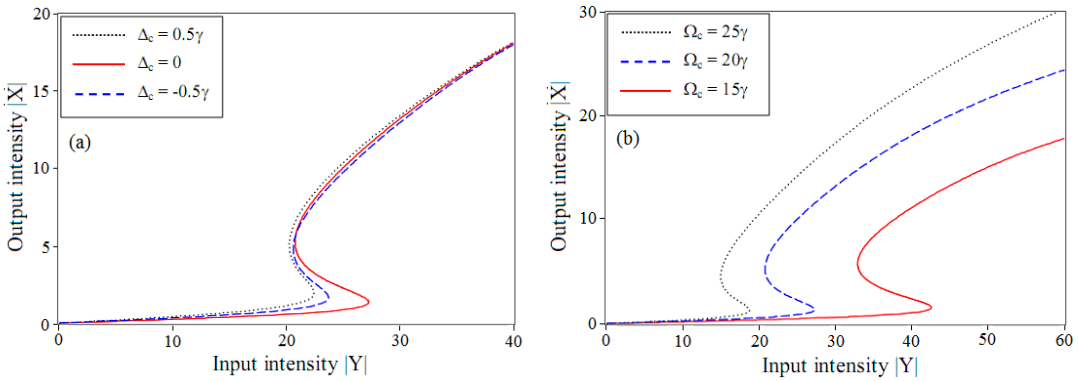

Fig. 29. The OB behavior at different values of frequency detuning (a) and intensity (b) of the coupling light when $C = 1000\gamma$ and $\Delta_p = -3\gamma$ [78].

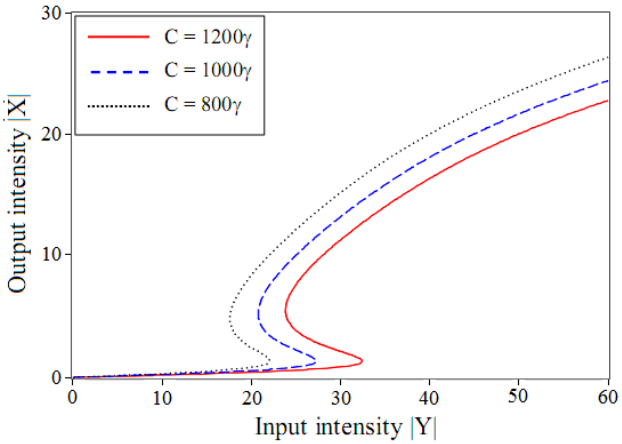

Fig. 30. Variation of OB at different values of the parameter C when Δ_p= -3γ, Ω_c= 20γ, and Δ_c= 0 [78].

The influence of the cooperation parameter C on OB behavior is presented in Fig. 30 for different values of the parameter C when Δ_p= 6γ, Ω_c= 10γ, and Δ_c= 0. It is apparent to see that

growing the cooperative parameter leads to increasing width of switching thresholds and lowering output intensity of the upper branch of OB curve. Such behaviors are attributed to C, which is proportional to atomic density: $C = N\omega_p L d_{21}^2/2c\varepsilon_0\hbar T$. Physically, an increase of C leads to an increase of absorption for the probe light, thus lowers upper branch of OB curve and requires a higher switching threshold.

VII. SUMMARY AND OUTLOOK FOR PERSPECTIVE

Absorption and dispersion are two basic properties of optical media which are mutually related through the Kramer-Kronig relationship. Under destructive interference of the total transition probability, the EIT effect occurs simultaneously with great enhancement of dispersion in the vicinity of the resonant region.

In the early years of EIT study, single EIT delivered a new interesting research topic and several related applications which were presented by a huge number of works and comprehensive reviews. However, the advent of multiple EIT with an analytical interpretation has gained additional advantages thus it has made recently a significant progress. At the time of writing this review (i.e., in 2018), we are some fourteen years from the first experimental demonstration of the multiple EIT in US [71] for a cold atomic medium in a magneto-optical trap. Since then, more effort has improved measurements to extend from cold to hot medium, which very recently (i.e., in 2017) is a nice measurement of multiple EIT spectrum and its dispersive profile performed in Vietnam [76]. There are constantly new and interesting proposals and demonstrations that extend multiple EIT to fresh applications. We have tried in this review to cover the works on multiple EIT and related applications. Whenever possible, we used analytical interpretations for usefulness of physics understanding and future applications. However, much work has been published in this topic, especially in the theoretical aspect, and it was simply not possible to cover or cite every single contribution. We humbly apologize to every one we have failed to cite.

Due to the simultaneous occurrence of EIT windows, it could be possible to generate entangled photons in quantum computing. Furthermore, due to controllable properties of dispersion, use of the multiple EIT medium is possible to manipulate and switch between subluminal and superluminal propagation modes in separated spectral regions. This behavior makes such medium useful for controlling multi-frequency light by a single-frequency light.

Along with controllable dispersion, giant Kerr nonlinearity occurred in separated spectral regions offers the multiple EIT media as a prototype candidate for nonlinear optics at low-light intensity. Furthermore, the switchable sign of Kerr nonlinearity can also be switchable between self-focusing and self-defocusing effects by the controlling laser field. Such giant Kerr nonlinearity and its switchable properties make the multiple EIT medium become active and more advantageous compared to the traditional nonlinear materials.

An apparent example for applications of multiple EIT, perhaps, is multi-channel OB. Indeed, giant Kerr nonlinearity delivers great OB sensitivity whereas its controllable magnitude and sign deliver controllable hysteresis loop which is fundamentally different from OB using traditional nonlinear optical materials. This is expected to make progress in high sensitivity and active photonics devices in near future such as optical switches, optical transistors, optical gates, and optical amplifiers. We also hope that the review will be useful for researchers understanding multi-window EIT and find farther ideas for future works.

ACKNOWLEDGMENT

The financial support from Vietnam Ministry of Science and Technology through the grant code ĐTĐLCN.17/17 is acknowledged.

REFERENCES

[1] A. Imamoglu, S. E. Harris, *Opt. Lett.* **14** (1989) 1344.
[2] K. J. Boller, A. Imamoglu, S. E. Harris, *Phys. Rev. Lett.* **66** (1991) 2593.
[3] Yong-qing Li and Min Xiao, *Phys. Rev. A* **51** (1995) 2703.
[4] Yong-qing Li and Min Xiao, *Phys. Rev. A* **51** (1995) 576.
[5] S. A. Hopkins, E. Usadi, H. X. Chen, A. V. Durrant, *Opt. Comm.* **138** (1997) 185.
[6] G. Welch, G. Padmabandu, E. Fry, M. Lukin, D. Nikonov, F. Sander, M. Scully, A. Weis, F. Tittel, *Found. Phys.* **28** (1998) 621.
[7] Jason J. Clarke and William A. van Wijngaarden, *Phys. Rev. A* **64** (2001) 023818.
[8] A. S. Zibrov, *Phys. Rev. A* **65** (2002) 043817.
[9] J. Zhao, L. Wang, L. Xiao, Y. Zhao, W. Yin, S. Jia, *Opt. Comm.* **206** (2002) 341.
[10] V. Ahufinger, R. Corbalan, F. Cataliotti, S. Burger, F. Minardi, C. Fort, *Opt. Comm.* **211** (2002) 159.
[11] H. S. Mon, L. Lee and J. B. Kim, *J. Opt. Soc. Am. B* **22** (2005) 2529.
[12] Li Li, P. Qi, A. Lazoudis, E. Ahmed, A. M. Lyyra, *Chem. Phys. Lett.* **403** (2005) 262.
[13] Y. Wu and X. Yang, *Phys. Rev. A* **71** (2005) 053806.
[14] S. Sen, T. K. Dey, M. R. Nath and G. Gangopadhyay, *J. Mod. Opt.* **62** (2015) 166-174.
[15] Hoonsoo Kang, Jong Su Kim, Sung In Hwang, Young Ho Park, Do-kyeong -Ko, Jongmin Lee, *Opt. Exp.* **16** (2008) 15728.
[16] S. Usefadeh and M. J. Karrimi, *Optik* **127** (21) (2016) 10208-10215.
[17] Yi-Wen Jiang, Ka-Di Zhu, Zhuo-Jie Wu, Xiao-Zhong Yuan and Ming Yao, *J. Phys. B: At. Mol. Opt. Phys.* **39** (12) (2006) 2612.
[18] V. Pavlovic, M. Susnjar, K. Petrovic, L. Stevanovic, Opt. Mat. **78** (2018) 191-200
[19] Rana Asgari Sabet, Mostafa Sahrai and Hamed Sattari, *App. Opt.* **56** (8) (2017) 7944-7951
[20] A. S. Zibrov, M.D. Lukin, D. E. Nikonov, L. Hollberg, M. O. Scully, V.L. Velichansky and H. G. Robinson, *Phys. Rev. Lett*. **75** (1995) 1499.
[21] A. Krishna, K. Pandey, A. Wasan and V. Natarajan, *Eur. Phys. Lett.* **72** (2005) 221.
[22] S. E. Harris, Lene Vestergaard Hau, *Phys. Rev. Lett.* **82** (1999) 4611.
[23] H. Schmidt and A. Imamoglu, *Opt. Lett*. **21** (1996) 1936.
[24] Hoonsoo Kang and Yifu Zhu, *Phys. Rev. Lett.* **91** (2003) 093601.
[25] H. Wang, D. Goorskey and M. Xiao, *Phys. Rev. Lett.* **87** (2001) 073601.
[26] L. V. Doai, D. X. Khoa, N. H. Bang, *Phys. Scr.* **90** (2015) 045502.
[27] A. Joshi, A. Brown, H. Wang and M. Xiao, *Phys. Rev. A* **67** (2003) 041801(R).
[28] S. E. Harris, J. E. Field and A. Kasapi, *Phys. Rev. A*. **46** (1) (1992) 29-32.
[29] Amitabh Joshi, Min Xiao, *Phys. Lett. A* **317** (2003) 370-377.
[30] M. Xiao, Y, -Q. Li, S. -Z. Jin, J. Gea-Banacloche, *Phys. Rev. Lett.* **74** (1995) 666.
[31] L.V. Hau, S. E. Harris, Z, Dutton, C.H. Bejroozi, *Nature* **397** (1999) 594.
[32] D. F. Phillips, A. Fleischhauer, A. Mair and R. L. Walsworth, *Phys. Rev. Lett.* **86** (2001) 783.
[33] S. E. Harris and Z. F. Luo, *Phys. Rev. A* **52** (1995) R928.
[34] D. X. Khoa, H. M. Dong, L. V. Doai and N. H. Bang, *Optik* **131** (2017) 497.
[35] H. M. Dong, L. V. Doai and N. H. Bang, *Opt. Comm.* **426** (2018) 553-557
[36] B. S. Ham, *J. Mod. Opt.* **49** (2002) 2477.
[37] M. A. Anton, F. Carreno, Oscar G. Calderon, S. Melle, I. Gonzalo, *Opt. Comm*, **281** (2008) 6040.
[38] Sabir Ali, Ayan Ray and Alok Chakrabarti, *Eur. Phys. J. D* **70** (2016) 27.
[39] T. Chaneliere, D. N. Matsukevich, S. D. Jenkins, S.-Y. Lan, T. A. B. Kennedy and A. Kuzmich, *Nature* (London) **438** (2005) 833.
[40] F. Vewinger, J. Appel, E. Figuera and A. Lvovsky, *Opt. Lett.* **32** (2007) 2771.

[41] D. McGloin, D. J. Fullton, M. H. Dunn, *Opt. Commu.* **190** (2001) 221.
[42] E. Paspalakis and P. L. Knight, "Electromagnetically induced transparency and controlled group velocity in a multilevel system", *Phys. Rev. A* **66** (2002) 015802.
[43] Y. Chen, X. G. Wei and B. S. Ham, *J. Phys. B: At. Mol. Opt. Phys.* **42** (2009) 065506.
[44] B.P. Hou, S.J. Wang, W.L. Yu, W.L. Sun, *Phys. Lett. A* **352** (2008) 462.
[45] J. Qi, *Phys. Scr.* **81** (2010) 015402.
[46] Y. Hong, Y. Dong, Z. Mei, F. Bo, Z. Yan and W.J, Hui, *Chin. Phys. B* **21** (11) (2012) 114207.
[47] H. Yu, K. S. Kim, J. D. Kim, H. K. Lee and J. B. Kim, *Phys. Rev. A* **84** (2011) 052511.
[48] Hoon Yu, Kwan Su Kim, Jung Dong Kim, Hyun Kyung Lee and Jung Bog Kim, *Phys. Rev. A* **84** (2011) 052511.
[49] Wenchao Xu and Brian DeMarco, *Phys. Rev. A* **93** (2016) 011801.
[50] A. Krasteva, B. Ray, D. Slavov, P. Todorov, P. N. Ghosh, S. Mitra and S. Cartaleva, *J. Phys. B: At. Mol. Opt. Phys.* **47** (2014) 175004.
[51] R. Kumar, V. Gokhroo and S.N. Chormaic, *New J. Phys.* **17** (2015) 123012.
[52] Fam Le Kien, *Phys. Rev. A* **91** (2015) 053847.
[53] S. Li, X. Yang, X. Cao, C. Xie and H. Wang, *J. Phys. B: At. Mol. Opt. Phys.* **40** (2007) 3211–3219.
[54] S. Bao, W. Yang, H. Zhang, L. Zhang, J. Zhao and S. Jia, *J. Phys. Soc. Jap.* **84** (2015) 104301.
[55] A. Jagannathan, N. Arunkumar, J. A. Joseph and J. E. Thomas, *Phys. Rev. Lett.* **116** (2016) 075301
[56] D. Han, Y. Zeng, Y. Bai, H. Cao, W. Chen, C. Huang, H. Lu, *Opt. Comm.* **281** (2008) 4712-4714.
[57] K. Yadav, A. Wasan, ' *Phys. Lett. A* **381** (2017) 3246-3253.
[58] V. Bharti, V. Natarajan, *Opt. Comm.* **392** (2017) 180-184.
[59] H. Sun, Y. Niu, S. Jin and S. Gong, *J. Phys. B: At. Mol. Opt. Phys*. **41** (2008) 065504.
[60] J. Sheng, X. Yang, H. Wu and M. Xiao, *Phys. Rev. A* **84** (2011) 053820.
[61] H. R. Hamedi and G. Juzeliunas, *Phys. Rev. A* **91** (2015) 053823.
[62] M. Sahrai, H.R. Hamedi and M. Memarzadeh, *J. Mod. Opt.*, **59** (11) (2012) 980–987.
[63] H. R. Hamedi, S. H. Asadpour, M. Sahrai, B. Arzhang, D. Taherkhani, *Opt Quant Electron*. **45**, (3) (2013) 295-306.
[64] L. Ebrahimi Zohravi, R. Doostkam, S. M. Mousavi and M. Mahmoudi, *Progr. in Electromag. Res. M* **25** (2012) 1-11.
[65] H. Jafarzadeh, *J. App. Phys*. **117** (2015) 163103.
[66] M. A. Antón, F. Carreño, O. G. Calderón, S. Melle and I. Gonzalo, *Opt. Commun.* **281** (2008) 6040.
[67] Yu R, Li J, Huang P, Zheng A, Yang X, *Phys. Lett. A* **373** (2009) 2992.
[68] A. Fountoulakis, A. F. Terzis and E. Paspalakis, *Phys. Lett. A* **374** (2010) 3354.
[69] Yu R, Li J, Ding C, Yang X, *Opt. Commun*. **284** (2011) 2930.
[70] Y. Li, C. Hang, L. Ma, G. Huang, *Phys. Rev. A* **354** (2006) 1.
[71] J. Wang, L.B. Kong, X.H. Tu, K.J. Jiang, K. Li, H.W. Xiong, Y. Zhu, M.S. Zhan, Phys. Lett., A 328, (2004) 437.
[72] K. Kowalski, , V. Cao Long, H. Nguyen Viet, S. Gateva, M. GÍódz, J. Szonert, *J. Non-Crystall. Solids* **355** (2009) 1295-1301.
[73] M.D. Lukin, A. Imamoglu, "Nonlinear Optics and Quantum Entanglement of Ultraslow Single Photons", *Phys. Rev. Lett*. **84** (2000) 1419.
[74] L.V. Doai, P.V. Trong, D.X. Khoa and N.H. Bang, *Optik*, **125** (2014) 3666–3669.
[75] D. X. Khoa, P. V. Trong, L. V. Doai and N. H. Bang, *Phys, Scr.* **91** (2016) 035401.
[76] D.X. Khoa, L.C. Trung, P.V. Thuan, L.V. Doai and N.H. Bang, *J. Opt. Soc. Am. B* **34** (2017) 1255.
[77] D. X. Khoa, L. V. Doai, D. H. Son and N. H. Bang, *J. Opt. Soc. Am. B* **31** (6) (2014) 1330.
[78] D. X. Khoa, L. V. Doai, L. N. M. Anh, L. C. Trung, P. V. Thuan, N. T. Dung and N. H. Bang, *J. Opt. Soc. Am. B* **33** (4) (2016) 735-740.
[79] R. Kumar, V. Gokhroo and S. N. Chormaic, *New J. Phys*. **17** (2015) 123012.
[80] Anh Nguyen Tuan, Doai Le Van, Son Doan Hoai and Bang Nguyen Huy, *Optik* **171** (2018) 721.
[81] N. T. Anh, L. V. Doai and N. H. Bang, *J. Opt. Soc. Am. B* **35** (2018) 1233.
[82] A. Lezama, S. Barreiro and A. M. Akulshin, *Phys. Rev. A* **59** (1999) 4732.
[83] M Fleischhauer, A Imamoglu and J P Marangos, *Rev. Mod. Phys.* **77** (2005) 633.
[84] J. P. Marangos, *J. Mod. Opt.* **45** (1998) 471.
[85] V. Tikhonenko, J. Christou and B. Luther-Davies, *Phys. Rev. Lett.* **76** (1996) 2698.

[86] Y. Li and M. Xiao, *Opt. Lett.* **21** (1996) 1064.
[87] M.D. Lukin, S.F. Yelin and M. Fleischhauer, *Phys. Rev. Lett*. **84** (2000) 4232.
[88] Hsiang-Yu Lo, Yen-Chun Chen, Po-Ching Su, Hao-Chung Chen, Jun-Xian Chen, Ying-Cheng Chen, Ite A. Yu and Yong-Fan Chen, Phys. Rev. A 83 (2011) 041804(R).
[89] X. Yang, S. Li, C. Zhang and H. Wang, *J. Opt. Soc. Am. B* **26** (7) (2009) 1423.
[90] M. Fleischhauer and M. D. Lukin, *Phys. Rev. Lett.* **84** (2000) 5094
[91] M. D. Lukin, *Rev. Mod. Phys*. **75** (2003) 457-472
[92] R. W. Boyd, D. J. Gauthier, A. L. Gaeta and A. E. Willner, *Phys. Rev. A* **71** (2005) 023801.
[93] R. W. Boyd, *J. Mod. Opt.* **56** (2009) 1908.
[94] M.M. Kash, V.A. Sautenkov, A.S. Zibrov, L. Hollberg, G.R. Welch, M.D. Lukin, Y. Rostovtsev, E.S. Fry, M.O. Scully, *Phys. Rev. Lett.* **82** (1999) 229.
[95] D. Budker, D. F. Kimball, S. M. Rochester, V.V. Yashchuk, *Phys. Rev. Lett.* **83** (1999) 1767.
[96] A. V. Turukhin, V.S. Sudarshanam, M. S. Shahriar, J. A. Musser, B. S. Ham, P.R. Hammer, *Phys. Rev. Lett*. **88** (2002) 023602.
[97] K. Bencheikh, E. Baldit, S. Briaudeau, P. Monnier, J. A. Levenson and G. Mélin, *Opt. Express* **18** (2010) 25642.
[98] L. J. Wang, A. Kuzmich and A. Dogariu, *Nature* **406** (2000) 277–279.
[99] E. E. Mikhailov, V. A. Sautenkov, I. Novikova, G.R. Welch, *Phys. Rev. A* **69** (2004) 063808.
[100] E. E. Mikhailov, V. A. Sautenkov, Y.V. Rostovtsev, G.R. Welch, *J. Opt. Soc. Am. B* **21** (2004) 425.
[101] A. M Akulshin and R. J McLean, *J. Opt.* **12** (2010) 104001.
[102] G. S. Agarwal, T. N. Dey, S. Menon, *Phys. Rev. A* **64** (2001) 053809
[103] K. Kim, H. S. Moon, C. Lee, S. K. Kim and J. B. Kim, *Phys. Rev. A* **68** (1) (2003) 013810.
[104] H. Sun, H. Guo, Y. Bai, D. Han, S. Fan, X. Chen, *Phys. Lett. A* **335** (2005) 68.
[105] M. Mahmoudi, M. Sahrai, H. Tajalli, *Phys. Lett. A* **357** (2006) 66.
[106] F. Carreño, Oscar G. Calderón, M. A. Antón and Isabel Gonzalo, *Phys. Rev. A* **71** (2005) 063805.
[107] I. H. Bae and H. S. Moon, *Phys. Rev.* A **83** (5) (2011) 053806.
[108] K. Qian, L. Zhan, L. Zhang, Z. Q. Zhu, J. S. Peng, Z. C. Gu, X. Hu, S. Y. Luo and Y. X. Xia, *Opt. Lett.* **36** (12) (2011) 2185.
[109] S. Dutta, *Phys. Scr.* **83** (2011) 015401.
[110] M. J. Akram, M. M. Khan and F. Saif, *Phys. Rev. A* **92** (2015) 023846
[111] T. N. Dey and G.S. Agarwal, *Phys. Rev.* A **76**, 015802 (2007).
[112] H. Ali, Ziauddin and I. Ahmad, *Laser Phys.* **24** (2014) 025201.
[113] H. Wu and M. Xiao, *Opt. Lett.* **32** (2007) 3122-3124.
[114] L.A. Lugiato, *Progr. in Opt.* **21** (1984) 71.
[115] H. M. Gibbs, *Optical Bistability: Controlling Light with Light*, Academic Press, New York, 1985.
[116] Hai Wang, David Goorskey and Min Xiao, *Opt. Lett*. **27** (15) (2002) 1354-356.
[117] A. Joshi, A. Brown, H. Wang and M. Xiao, *Phys. Rev. A* **67** (2003) 041801(R).
[118] M A Anton and Oscar G Calderon, *J. Opt. B: Quantum Semiclass. Opt.* **4** (2002) 91–98.
[119] A. Joshi and M. Xiao, *Phys. Rev. Lett.* **91** (2003) 143904.
[120] A. Joshi, A. Brown, H. Wang and M. Xiao, *Phys. Rev. A* **67** (2003) 041801(R).
[121] J. Li, *Physic. D* **228** (2007) 148.
[122] Zhen Wang, Ai-Xi Chen, Yanfeng Bai, Wen-Xing Yang and Ray-Kuang Lee, *J. Opt. Soc. Am. B* **29** (10) (2012) 2891-2896.
[123] J. H. Li, X. Y. Lu, J. M. Luo and Q. J. Huang, *Phys. Rev. A* **74** (2006) 035801.
[124] X. Y. Lu, J. H. Li, J. B. Liu and J. M. Luo, *J. Phys. B,* **39** (2006) 5161.
[125] M. Sahrai, S.H.Asadpour, H.Mahrami and R.Sadighi-Bonabi, *J. Lumines.* **131** (2011) 1682–1686.
[126] M. Sahrai, H.R. Hamedi and M. Memarzadeh, *J. Mod. Opt.* **59** (2012) 980.
[127] H. R. Hamedi, S. H. Asadpour, M. Sahrai, B. Arzhang, D. Taherkhani, *Opt. Quant. Electron.* **45** (2013) 295.
[128] L. Ebrahimi Zohravi, R. Doostkam, S. M. Mousavi and M. Mahmoudi, *Progr. Electromag. Re. M*. **25** (2012) 1.